nature neuroscience

Precision and diversity in an odor map on the olfactory bulb

Edward R Soucy[1,2], Dinu F Albeanu[1,2], Antoniu L Fantana[1], Venkatesh N Murthy[1] & Markus Meister[1]

We explored the map of odor space created by glomeruli on the olfactory bulb of both rat and mouse. Identified glomeruli could be matched across animals by their response profile to hundreds of odors. Their layout in different individuals varied by only ~1 glomerular spacing, corresponding to a precision of 1 part in 1,000. Across species, mouse and rat share many glomeruli with apparently identical odor tuning, arranged in a similar layout. In mapping the position of a glomerulus to its odor tuning, we found only a coarse relationship with a precision of ~5 spacings. No chemotopic order was apparent on a finer scale and nearby glomeruli were almost as diverse in their odor sensitivity as distant ones. This local diversity of sensory tuning stands in marked distinction from other brain maps. Given the reliable placement of the glomeruli, it represents a feature, not a flaw, of the olfactory bulb.

In many regions of the brain, neurons form an ordered representation of the outside world, as exemplified by the 'homunculus' of the somatosensory cortex, a point-to-point topographic map of the body surface onto the brain surface. There has been great interest in such a systematic relationship between the function of neurons and their anatomical arrangement, as the map can suggest what processing the circuit performs[1,2]. Most brain computation is local, relying on short connections between nearby cells[3]. This is a necessity, as the connections between neurons occupy most of the volume available to the brain, and long-distance connections require more volume. Consequently, the arrangement of neurons in a given brain region constrains which neuronal signals can be brought together in subsequent computations. Here we analyzed a sensory map in the olfactory system, namely the two-dimensional arrangement of glomeruli on the olfactory bulb.

Olfaction begins at the olfactory epithelium, which lines the upper region of the nasal cavity, where millions of receptor cells transduce the binding of odorous molecules into a neural signal. The genomes of the rat and the mouse contain ~1,000 genes for odorant receptors, but each sensory neuron is thought to express only one gene from this large set[4]. This results in ~1,000 types of receptor neurons that are broadly intermixed on the epithelium[5]. Receptor neurons send their axons to the olfactory bulb, where they undergo a marked resorting. Axons from a particular receptor neuron type converge onto a tight focus and their terminals form a glomerulus. About 2,000 glomeruli line the outer shell of the left and right olfactory bulbs; generally one finds two glomeruli for each receptor type[6,7].

The positioning of glomeruli follows certain general rules. There is approximate mirror symmetry between the left and right bulbs, in that glomeruli innervated by the same receptor neuron type appear to be reflected across the sagittal midplane of the brain[8–10]. Across animals, the layout of glomeruli appears to be similar, but not identical[11–14]. Furthermore, there is some relationship between the spatial position of a glomerulus and its odor sensitivity. Certain domains of the bulb respond preferentially to specific odor classes[15–17]. There have been suggestions of even more detailed structure: in a given odor class, glomeruli that are responsive to structurally similar molecules have a tendency to lie close to each other[9,10,18–20]. This has been termed a 'chemotopic map'.

The goals of this study were twofold: to determine the precision of the olfactory map on the bulb and to understand how the map relates to odor processing. We began by identifying the functional properties of each glomerulus, defined by its sensitivity spectrum to a large panel of odors. We found that this functional identification alone allowed us to uniquely tag many glomeruli in both rat and mouse. On that basis, we asked how reproducible the two-dimensional arrangement of these glomeruli is, which would reveal the accuracy with which Nature has established this neuronal map. We then tested whether there was indeed a systematic functional relationship among nearby glomeruli on the olfactory bulb.

RESULTS

We measured neural activity in glomeruli of the olfactory bulb in response to large panels of odors using two different optical reporters (**Fig. 1**): the intrinsic signal and synaptopHluorin (SpH). Both techniques allow for extended recordings without degradation of the signal, as they require no exogenous indicators. The intrinsic signal can be used in all species, whereas the SpH method relies on a genetic construct that is currently restricted to mice. On the other hand, the SpH probe delivers much stronger optical signals. Given these complementary benefits and

[1]Department of Molecular and Cellular Biology and Center for Brain Science, Harvard University, 52 Oxford Street, Cambridge, Massachusetts 02138, USA. [2]These authors contributed equally to this work. Correspondence should be addressed to M.M. (meister@fas.harvard.edu) or V.N.M. (vnmurthy@fas.harvard.edu).

Received 24 September 2008; accepted 18 December 2008; published online 18 January 2009; doi:10.1038/nn.2262

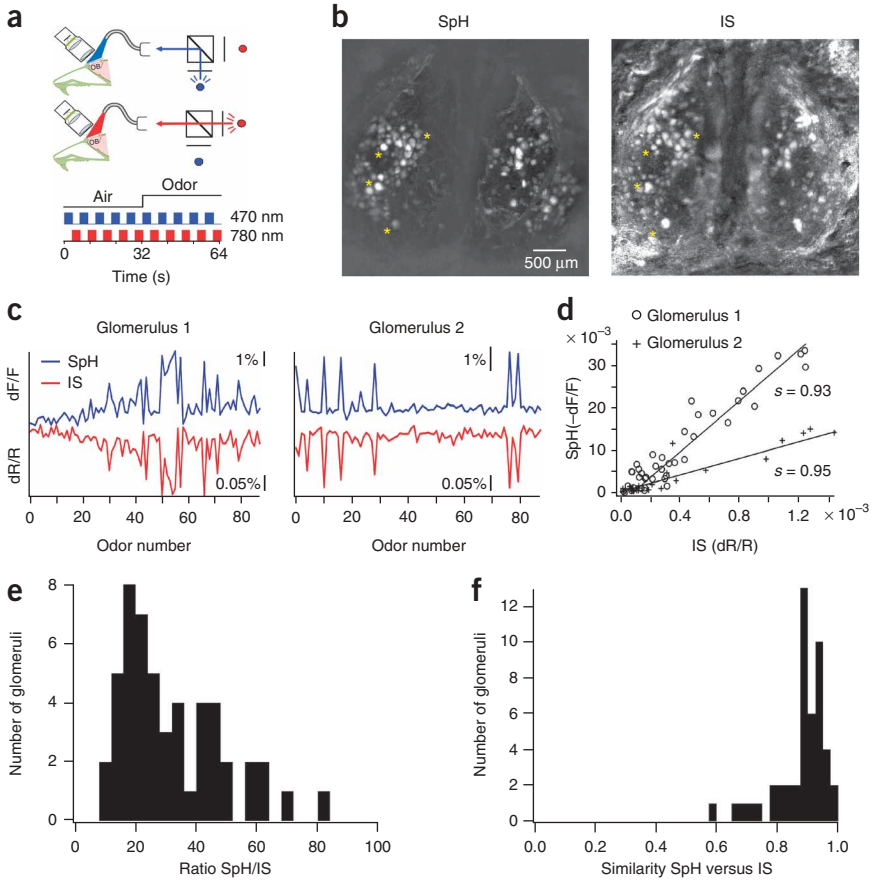

Figure 1 SpH and intrinsic signal report the same odor dependence. (**a**) Experimental setup. The surface of the olfactory bulb was imaged with a CCD camera. A dual beam illuminator allowed interleaved illumination with blue or red light to acquire both SpH and intrinsic optical signals during the same odor response. (**b**) Maximum-intensity projection images of odor responses on the olfactory bulbs of a SpH-transgenic mouse, probed by SpH fluorescence (left) and the intrinsic signal (right). Each pixel was assigned the highest signal amplitude elicited by any of 88 odor stimuli. Approximately 70 glomeruli were stimulated effectively in each bulb. The sign of the intrinsic signals was inverted for ease of comparison. Asterisks mark reference points in the two images. (**c**) Comparison of responses from two glomeruli (left and right) to 88 odors, measured by the relative fluorescence change of SpH (dF/F) and the relative reflectance change of intrinsic signals (dR/R). For odor identities, see **Supplementary Tables 1** and **2**. (**d**) Scatter plot of the data shown in **c**. Note that SpH and intrinsic signal varied proportionally, but the slope is different for the two glomeruli. The correlation coefficient (*s*) between the two signals is listed for each glomerulus. (**e**) The ratio of SpH to intrinsic signal, shown as a histogram for 51 glomeruli. For each glomerulus, the ratio was determined from the slope in the plot of **d**. (**f**) Histogram of the correlation coefficient (see **d**) for all 51 glomeruli.

our desire to compare results from mice and rats, we used both techniques. In early experiments, we applied both methods simultaneously to the same glomeruli and found that they reported the same spectrum of odor responses (see Methods and **Fig. 1**).

Glomeruli can be identified reliably by their odor response

Given a large enough set of odorants, one expects that each glomerulus will have a unique response spectrum, governed by the ligand-binding affinities of the corresponding olfactory receptor protein, with possible contributions from lateral signal flow in the bulb. If so, one might be able to recognize a glomerulus with the same receptor type purely by its odor responses. The bilateral symmetry of receptor neuron projections to the two bulbs provides a test of this proposition because one expects to find glomeruli with identical odorant sensitivity at approximately mirror-symmetric locations across the midplane.

We examined this matching process with a small patch of glomeruli in the two olfactory bulbs of a mouse (**Fig. 2a**). All of these were activated by the same odor, and from this stimulus alone, it was unclear how glomeruli on the left bulb should be matched with those on the right (**Fig. 2b**). Under stimulation with other odors, however, the glomeruli in this patch differed greatly in their responses and each had a unique odor spectrum. Moreover, each odor spectrum on the left side had a near perfect match on the right side (**Fig. 2c**). On occasion, we found several possible matches of equivalent quality (**Fig. 2c**), perhaps resulting from duplicate glomeruli with the same odorant receptor[12]. We avoided such ambiguous assignments by requiring a unique match (see Methods) and excluded the respective glomeruli from further analysis.

We tested whether this functional label for a glomerulus corresponds to the molecular label provided by its olfactory receptor type. A transgenic mouse line in which the M72 olfactory receptor is fluorescently tagged[21] showed a single fluorescent glomerulus on the dorsal side of each bulb (**Fig. 3a**). This glomerulus was strongly activated by several tiglate odorants (**Fig. 3b**). Other glomeruli nearby shared some sensitivity to tiglates, but differed in other parts of the odor spectrum (**Fig. 3b,c**). We used the measured odor spectrum of M72 in one animal as a template to search blindly for a match in other animals. For every target glomerulus, we computed the correlation between its odor spectrum and the template (equation (1)). The peak correlation value reliably identified a single glomerulus in each animal (**Fig. 3c**) and the fluorescence image revealed that this glomerulus was indeed innervated by the M72 receptor (confirmed in 10 out of 10 pairs of bulbs). We conclude that the odor spectrum is a reliable tag for the molecular identity of glomeruli.

A precise layout of identified glomeruli in mouse and rat

We applied the above correlation method to match glomeruli in two olfactory bulbs automatically by their odor spectra (see Methods). We matched 25 glomeruli between the two bulbs of the same mouse (**Fig. 4a**). Even though the method was entirely blind to the location of glomeruli, the resulting layout of matched glomeruli showed approximate mirror symmetry across the midline. To inspect the deviations from mirror symmetry, we overlaid and aligned the two patterns (**Fig. 4b**). This revealed that the shifts between the left and right glomerular layouts were not isotropic (**Fig. 4c**). The displacements of corresponding glomeruli were considerably larger in the antero-posterior direction (r.m.s. displacement = 139 µm, 141 pairs of glomeruli) than in the medio-lateral direction (95 µm). For reference, the average spacing between glomeruli in these animals was 108 µm.

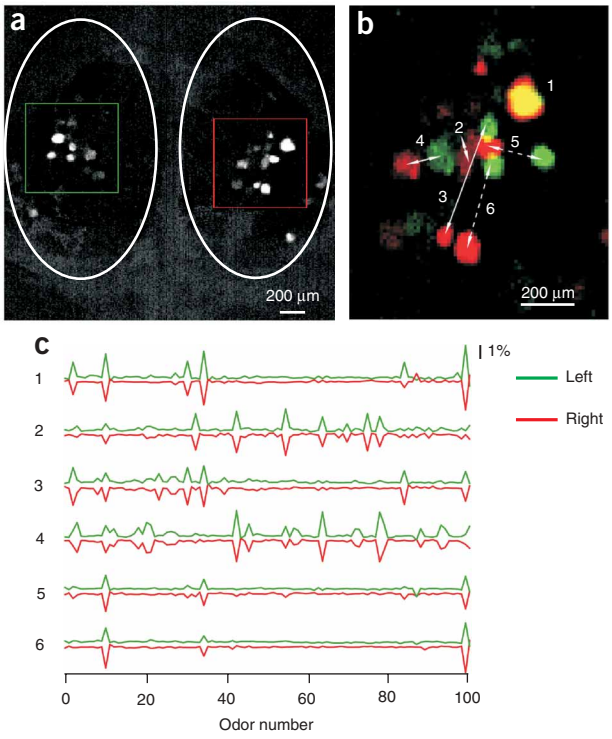

Figure 2 Glomeruli can be tagged by their odor responses. (**a**) The activation pattern in both bulbs of one mouse, induced by the odor ethyl tiglate and measured by SpH. (**b**) Overlay of the left bulb (green) and right bulb (red) from **a**. The left bulb image was reflected about the midline and shifted to align the glomeruli labeled 1. Arrows indicate pairs of glomeruli with matching odor response spectra (see Methods). (**c**) Responses to 100 odors for the six pairs of glomeruli labeled in **b**. The spectra for the right bulb glomeruli are inverted on the ordinate to facilitate the comparison. Note the assignment for glomeruli 5 and 6 was ambiguous, as all four members had very similar odor spectra. These cases did not pass the criterion for a unique match (see Methods) and were not used in further analysis (dashed arrows in **b**). For odor identities, see **Supplementary Table 1**.

We can conceive the actual layout of glomeruli in any given bulb as resulting from the 'prototype' layout, modified by errors in positioning that occur during development. When two such layouts are aligned, each bulb is affected independently by the positioning error. Thus, the displacement between matched glomeruli in the two layouts has a s.d. that is $\sqrt{2}$-fold larger than the error in each individual layout. From this, we found that the developmental variability in glomerular position relative to the prototype map was 98 µm (r.m.s.), or 0.9 spacings, in the antero-posterior direction and 67 µm, or 0.6 spacings, in the medio-lateral direction (**Table 1**). When comparing the bulbs of two different animals, the displacements of matching glomeruli were almost identical to those measured across bulbs in the same animal (**Fig. 4d** and **Table 1**).

We applied the same analysis of developmental precision to the rat (**Supplementary Fig. 1** online). Again, the odor spectra of glomeruli were quite diverse, but a glomerulus in one bulb often had a precisely matching odor spectrum in the opposite bulb, allowing a reliable assignment of corresponding glomeruli. The deviations from symmetry were measured as before. As in the mouse, we found a clear difference between the two anatomical axes, with ~two-fold larger displacements along the antero-posterior axis (**Fig. 4e** and **Table 1**). Again, we converted the measured displacements to the developmental error around the presumed prototype layout. Across animals, this scatter amounted to 1.6 glomerular spacings in the antero-posterior direction and 1.0 spacings in the medio-lateral direction (**Table 1**). The average spacing between rat glomeruli was 160 µm.

These measurements of map precision can provide constraints on models of axon guidance in the olfactory bulb. For example, two general scenarios could explain the variability in glomerular placement. In one scenario, the global gradients of axon guidance cues in the bulb vary from animal to animal, leading to slightly different layouts. Alternatively, the gradients are very reproducible and the noise arises when the receptor axons read those cues. The former hypothesis predicts that nearby glomeruli should vary less in their relative placement than distant glomeruli, as they target similar levels of the guidance molecules. We tested this and found no evidence for such an

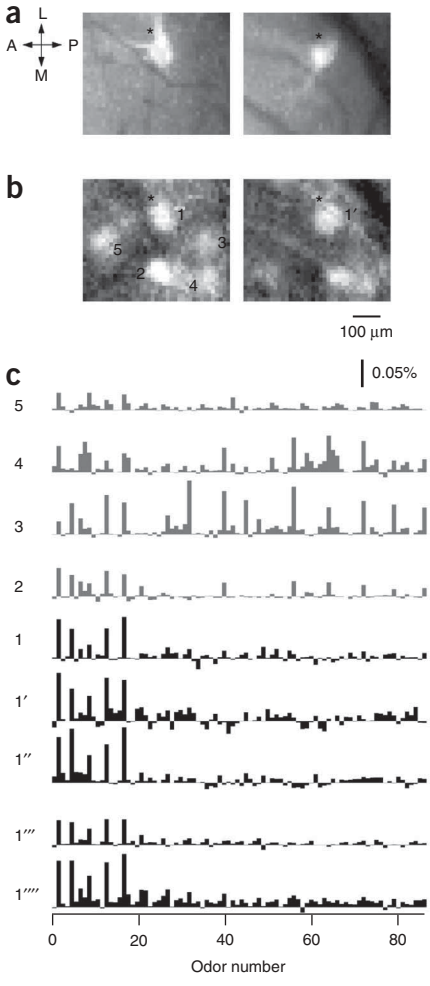

Figure 3 A genetically labeled glomerulus validates the tagging procedure. (**a**) Sensory axons with a fluorescent M72-GFP olfactory receptor identified a glomerulus on the posterior dorsal olfactory bulb in two different mice (left and right). (**b**) Intrinsic signal response to a single odor (isopropyl tiglate) in the same regions shown in a (see asterisks for alignment). Several glomeruli responded, including the M72 glomerulus (labeled 1 and 1′). (**c**) Response spectra to 85 odors for the M72 glomerulus (1) and neighboring ones in the same animal (2–5), as labeled in **b**. In another analysis, we selected an M72 glomerulus (spectrum 1‴) as a reference and found the glomeruli with the best matching response spectra in four other olfactory bulbs (1, 1′, 1″ and 1⁗). All four of these glomeruli were positive for M72-GFP. For odor identities, see **Supplementary Table 1**. A, anterior; L, lateral; M, medial; P, posterior.

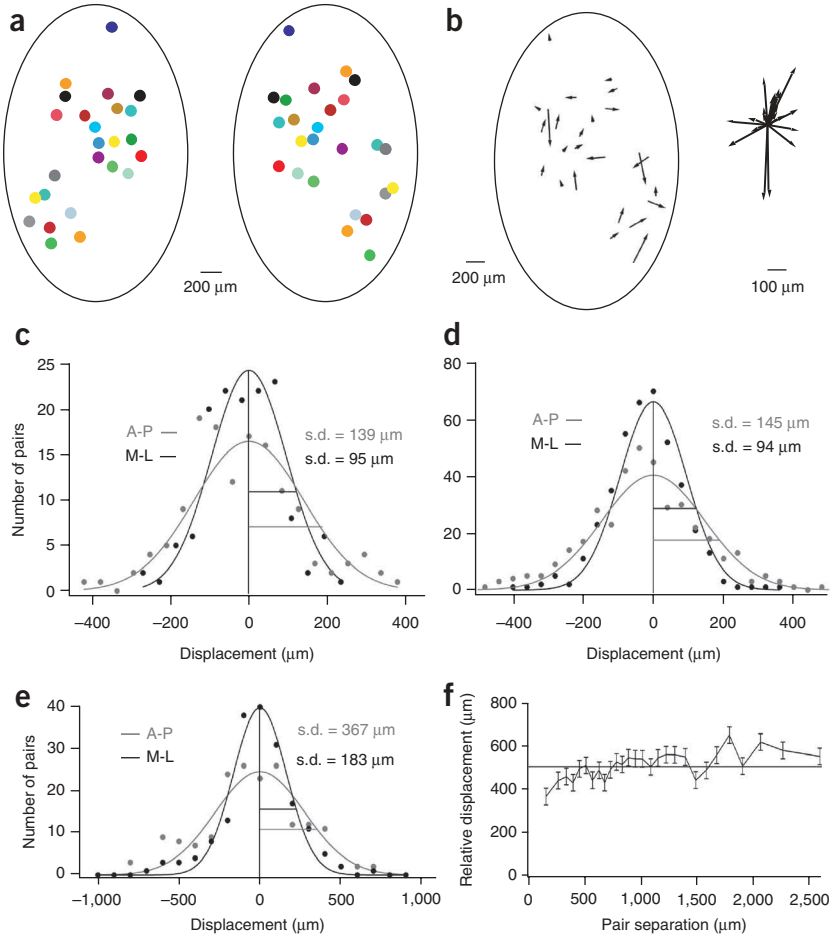

Figure 4 Mouse and rat glomeruli are positioned precisely. (**a**) Locations of odor-activated glomeruli on the two olfactory bulbs in one mouse. Odor spectra on the left bulb were matched with those on the right bulb and the 25 best matches are shown with colored circles. (**b**) To align the glomerular layouts in the two bulbs, we mirrored the left bulb onto the right, and rotated and translated the left bulb to minimize the displacement of matched pairs of glomeruli. Left, arrows indicate the resulting displacement vectors for all pairs of glomeruli from the location in the right layout to that in the left layout. Right, the same displacement vectors rooted on a common origin. (**c**) Histogram of glomerular displacements between left and right bulbs of the same mouse (141 pairs in ten mice) measured separately along the anterior-posterior (A-P) and the medial-lateral (M-L) direction. Curves are Gaussian fits centered on the origin, with s.d. as quoted. (**d**) A histogram of glomerular displacements across bulbs of different mice (412 pairs in five mice) is shown, displayed as in **c**. (**e**) A histogram of glomerular displacements between left and right bulbs of the same rat (202 pairs in seven rats) is shown, displayed as in **c**. (**f**) We tested whether nearby glomeruli suffer similar displacements in comparing the layouts of two bulbs. Plotted along the abscissa is the separation of two glomeruli in one bulb and along the ordinate is the change in this separation vector in the other bulb (202 glomeruli in seven rats; mean ± s.e.m., see Methods). The straight line indicates the average relative displacement for all pairs.

effect (**Fig. 4f**). This result favors the latter hypothesis, which states that the variability arises at the read-out stage. Recent studies have provided evidence that two different mechanisms of axon guidance determine the antero-posterior and the dorso-ventral coordinates of a glomerulus[6,7]. Our observations of anisotropic precision suggest that the antero-posterior mechanism is less precise than the orthogonal one.

Some glomeruli have identical odor responses across species

Given the observed precision of glomerular placement, we can specify what the prototype map is for the identifiable glomeruli on the dorsal bulb (**Fig. 5**). Some of these glomeruli were recognized in almost every olfactory bulb that we inspected, whereas others were recognized in only a fraction. These differences were partly a result of anatomical variation in the dorsal viewing window and of imaging noise and a conservative selection procedure (see Methods). For the glomeruli that were encountered repeatedly, we determined the prototype layout in the mouse (31 glomeruli; **Fig. 5a**) and the rat (34 glomeruli; **Fig. 5b**) (the odor spectra that tag the identity of each of these canonical glomeruli are provided in **Supplementary Figs. 2** and **3** online).

Among the canonical glomeruli in the prototype maps for mouse and rat, we encountered ten whose odor spectra matched very well across species: to within the confidence limits developed for matches within a species (**Fig. 5c**). For almost all of these (9 out of 10 in mouse and 10 out of 10 in rat), the match to a glomerulus in the other species was better than to the most similar glomerulus in the same species. In a less restrictive procedure, we began by matching individual bulbs across species (see Methods). This method identified, in addition to the above ten, an additional six canonical glomeruli with near-identical spectra in mouse and rat (**Supplementary Fig. 4** online). These observations suggest that rat and mouse share a substantial fraction of olfactory receptors with very similar odor-binding sites.

Mouse and rat are separated by a large evolutionary distance, but their olfactory receptor genes are unusually similar: About one third of the receptor genes have an ortholog in the other species with >90% protein sequence identity, closer than the nearest paralog in the same species[22]. This suggests that there is some degree of selection pressure to maintain those sequences. Whether the sequence similarity translates to identical odor-binding spectra remains to be seen, but it is now possible to connect the odor spectrum of a glomerulus to the molecular identity of the underlying receptor[11] and this should allow further exploration of the conserved glomeruli and their ligands.

Notably, the matching glomeruli were also located at similar positions in the two species. To allow for the different anatomical size of the bulbs, we normalized the two prototype layouts by the average glomerular spacing (AGS) in each species. After this scaling, the layouts of matched glomeruli in the mouse and rat differed by only ~1.0 AGS in the medio-lateral direction and 3.9 AGS in the antero-posterior direction (**Fig. 5d** and **Table 1**). For comparison, if we chose pairs of glomeruli from the two maps at random, the scatter would be much greater: 4.4 AGS in medio-lateral and 8.8 AGS in antero-posterior. Clearly there is a strong correspondence between the respective map positions of functionally related glomeruli in mouse and rat. This comparison of functional anatomy in the bulb could be extended readily to other species using the intrinsic signal method, which requires no genetic modification.

Table 1 Summary of precision in the glomerular layout on the olfactory bulb

		Across hemispheres			Across animals		
		Number of pairs	Precision (μm)	Relative precision (AGS)	Number of pairs	Precision (μm)	Relative precision (AGS)
Mouse	A-P	141	98	0.9	412	103	1.0
	M-L	141	67	0.6	412	66	0.6
Rat	A-P	202	260	1.6	102	258	1.6
	M-L	202	131	0.8	102	156	1.0
Mouse-rat prototype	A-P	–	–	–	10	–	3.9
	M-L	–	–	–	10	–	1.0

The precision of placement of glomeruli is measured as 1 s.d. of the scatter about the average position in the layout and reported in either absolute units (precision) or multiples of the average glomerular spacing (relative precision). The results are reported separately by species (mouse versus rat), by condition (comparing two bulbs in the same animal or across animals), and by anatomical direction (antero-posterior (A-P) versus medio-lateral (M-L)), and the number of glomerular pairs contributing is listed in each case (number of pairs). The precision of alignment of the mouse and rat layouts is based on the ten canonical glomeruli in **Figure 5**.

A coarse-scale map from odor space onto the olfactory bulb

Above, we have discussed the developmental precision in the layout of glomeruli; we move now to the functional logic of their arrangement. Specifically, we would like to find a systematic relationship between the chemical sensitivity of a glomerulus and its position on the olfactory bulb. The prototype layouts described above (**Fig. 5**) provide a look-up table between odor spectrum and spatial location, but convey no understanding of the rules behind the layout.

Perhaps the simplest hypothesis for a mapping rule is a linear relationship between odor responses and position (equation (2)). In this map, each odor is assigned one location on the bulb. A hypothetical glomerulus that responds exclusively to one odor would be mapped to that odor's location. A glomerulus that responds to several odors is mapped to an intermediate position, determined by weighting each single-odor location with the response to that odor. This type of relationship between the responses and locations of neurons applies, at least locally, in many somatotopic or visuotopic maps in the brain.

Given the measured odor spectra and locations for all glomeruli, we derived the optimal linear map between the two (see Methods). To explore its utility, we began by focusing on the rat, as the larger bulb allows a more precise position measurement and prior work has elaborated odor maps extensively in this species[17,20]. We found that the linear map did provide some prediction as to where a glomerulus lies on the basis of the odor spectrum alone, but it was incomplete and coarse (**Fig. 6a**). Along the antero-posterior axis, the predicted position was correlated with the true position, but the discrepancy had a s.d. of ~600 μm, much greater than the inherent antero-posterior variability in the layout of glomeruli (260 μm; **Table 1**). Thus, the linear map does not account for the location of glomeruli to the accuracy with which they are arranged. Along the medio-lateral axis, which has a much shorter extent, the linear map was not useful at all: the errors in the predicted positions were almost as large as the range of positions.

How is the prediction of antero-posterior locations achieved? Inspection of the coefficients in the linear fit showed that only a small number of odors contributed to this (**Fig. 6b**). Furthermore, the subsets of odors that were assigned very anterior or very posterior positions each shared strong structural similarity. Among the pure compounds that predicted anterior placement of the glomerulus, aliphatic aldehydes made up four of the seven odors. All were straight-chain molecules containing a double-bonded oxygen species.

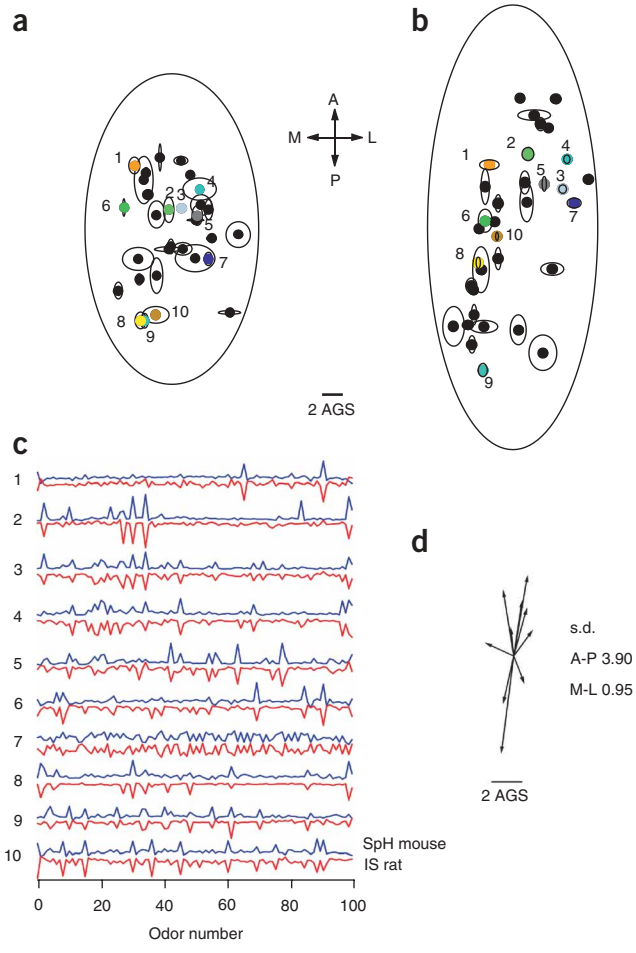

Figure 5 Prototype layout of glomeruli in mouse and rat. (**a**) Prototypical glomerular layout for the mouse. Circles indicate the average location on the bulb for 31 glomeruli that were reliably identified across experiments (based on eight bulbs). Circle diameter is equal to the average glomerular diameter. Ellipses indicate 1 s.d. of the scatter in position about the mean location. Colored circles and numbers label glomeruli that had matching odor spectra in mouse and rat (the odor spectra of these glomeruli are plotted in **Supplementary Fig. 2**). (**b**) Prototypical glomerular layout for the rat, identifying 34 glomeruli (based on four bulbs), displayed as in **a**, with the spatial scale normalized to the AGS. The odor spectra of these glomeruli are plotted in **Supplementary Fig. 3**. (**c**) Odor spectra of ten canonical glomeruli (colored dots in **a** and **b**) whose responses are almost identical in the mouse and rat. Glomerular activity was recorded using the SpH probe in the mouse and intrinsic signals in the rat. For odor identities, see **Supplementary Table 1**. (**d**) Displacement vectors between matched glomeruli in the mouse and rat layouts, rooted to a common origin and scaled in terms of the AGS.

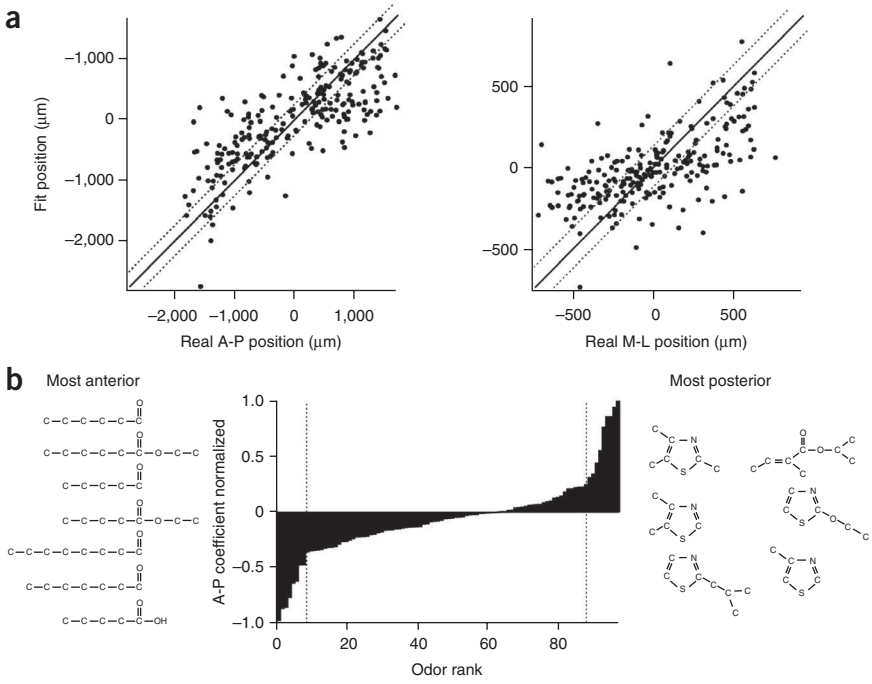

Figure 6 A coarse map relates the location of a glomerulus to its odor spectrum. (**a**) The optimal linear odor map for the rat olfactory bulb. The glomerular position as predicted by the optimal map (equation (2)) is plotted against the actual position. Solid line denotes the identity. Dotted lines represent the scatter (±1 s.d.) expected from the measured accuracy of glomerular placement, if the linear relationship accounted entirely for the chemotopic map. Note the actual scatter was much greater. Left, antero-posterior position; the fit has a correlation coefficient of $r^2 = 0.59$. Right, medio-lateral position; $r^2 = 0.42$. Data are from four bulbs in two rats. (**b**) The weighting coefficient (A_{1j} in equation (2)) for each odor response in fitting the antero-posterior position of the glomerulus. The odors are ordered by the strength of their coefficient. A few odors emerged with unusually strong anterior (negative) or posterior (positive) weights (outside dotted lines). Their chemical structures are shown on the left and right, respectively. For odor identities, see **Supplementary Table 1**.

In contrast, the odors that predicted a posterior placement were, with a single exception, thiazoles. Given that this odor set (**Supplementary Table 1** online) contained many other compounds, these structural similarities clearly stand out. Moreover, a second odor set (**Supplementary Table 1**) that did not contain these molecules allowed no systematic prediction of antero-posterior position. Thus, among the classes of odorants that we tested, the straight-chain hydrocarbons and the thiazoles produced responses that were clearly localized to one portion of the dorsal bulb.

We conclude that a linear map between odor spectrum and location of a glomerulus can account for coarse positioning to within ~5 glomerular spacings, but not on the finer scale of the natural precision of the layout. This analysis is consistent with previous reports that responses to certain odors can be preferentially localized to a 'domain' or 'module' of the dorsal bulb, typically ~1 mm in size[16,17,20,23].

Fine-scale diversity in the odor map

Closer inspection of the domains identified by the aldehydes or thiazoles showed that they still contained glomeruli with a great diversity of chemical spectra. For example, as in previous studies[10,19] we encountered some local clusters of glomeruli that were responsive to aldehydes (**Fig. 7a**). However, two glomeruli with similar responses over the aldehyde series often had very different responses to the remainder of the odor set (**Fig. 7b,c**). Furthermore, interspersed among the glomeruli responsive to aldehydes were glomeruli that were entirely insensitive to this class of odors (**Figs. 5** and **7b,c**). Similar heterogeneity was found in the domain associated with thiazoles. Is there any systematic odor dependence in these fine-scale arrangements?

The relationship between odor spectrum and the location of a glomerulus may conceivably be very convoluted and nonlinear, in which case a global linear fit to the map (**Fig. 6a**) will be only moderately successful. To the extent that there is a systematic relationship, however nonlinear, we still expect to find local order in the map: nearby glomeruli should have similar odor sensitivity spectra. We tested this prediction for the rat's glomerular layout by analyzing the relationship between physical distance and functional similarity among pairs of glomeruli.

To measure the functional similarity of two glomeruli, we used the same quantity that allowed their identification across animals, namely the correlation coefficient of their response spectra to a large set of

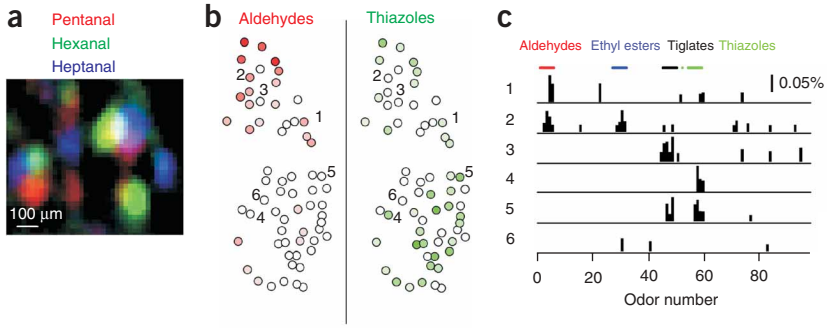

Figure 7 Local diversity in the map of glomeruli. (**a**) Detail of odor responses in a small region of the rat olfactory bulb. In each pixel, the response amplitudes to aliphatic aldehydes of three different chain lengths (pentanal, hexanal and heptanal) are encoded with the red, green and blue color channels. The local clusters of glomeruli that are each tuned sharply to adjacent chain lengths should be noted. (**b**) Glomeruli on one olfactory bulb of a rat. Sensitivity to aliphatic aldehydes is marked in red (left) and sensitivity to thiazoles in green (right). (**c**) Odor response spectra of selected glomeruli labeled in **b**; note the sensitivity to aldehydes in the anterior and to thiazoles in the posterior bulb. Adjacent glomeruli can have nonoverlapping odor spectra (for example, 4 and 6). The aldehyde 'domain' included glomeruli with no sensitivity to those odors (for example, 3). Glomeruli with overlapping sensitivity to aldehydes may have entirely different responses to other odors (for example, 1 and 2). For odor identities, see **Supplementary Table 1**.

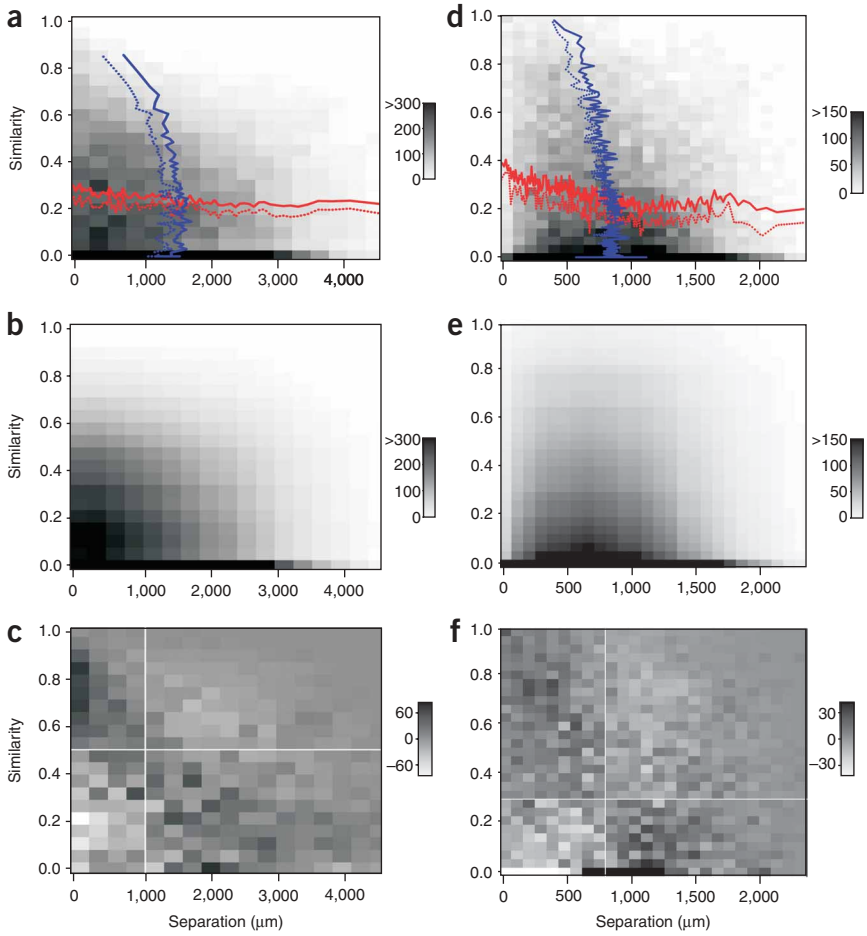

Figure 8 Lack of local chemotopy. (**a**) Relationship between the odor response similarity (ordinate, equation (1)) of two glomeruli and their spatial separation (abscissa) in the rat. The analysis extended over 31,510 pairs of glomeruli in 14 olfactory bulbs from 7 rats. Each pair of glomeruli contributed one count in this histogram and the gray scale reports the number of counts in each bin. Red lines indicate mean (solid) and median (dashed) similarity versus distance, obtained by binning the distance. Blue lines indicate mean (solid) and median (dashed) distance versus similarity, obtained by binning the similarity. For odor identities, see **Supplementary Table 1**. (**b**) Under the null hypothesis in which there is no chemotopy whatsoever, the response similarity of a pair of glomeruli should have the same probability distribution at all distances. Therefore, the joint distribution of similarity and distance should equal the product of the two marginal distributions (see Methods). This prediction is plotted here; note the close resemblance to the measured distribution (**a**). (**c**) Difference between the measured distribution (**a**) and the distribution expected in the absence of any chemotopy (**b**), plotted on an expanded grayscale. The region with the strongest deviation from the null hypothesis included the pairs separated by <1 mm (vertical line) with similarity of >0.5 (horizontal line). (**d**) Distribution of response similarity and spatial separation for glomeruli in the mouse, presented as in a. Data are from 33,169 pairs of glomeruli in 20 bulbs from 10 mice. For odor identities, see **Supplementary Table 1**. (**e**) Distribution expected under the null hypothesis of no chemotopy, presented as in **b**. (**f**) Difference between the measured distribution (**d**) and the distribution expected in absence of any chemotopy (**e**), presented as in **c**. The strongest deviation appeared for pairs of glomeruli separated by <0.7 mm (vertical line) with similarity of >0.3 (horizontal line).

odors (equation (1)). This is a natural choice because it directly measures the overlap between the molecular receptive ranges[24] of the two glomeruli; in turn, the receptive range overlap has been cited as a criterion for chemotopic order on the olfactory bulb[25]. Furthermore, a very similar correlation coefficient has been in common use for assessing the similarity of odor response patterns[16].

With this similarity measure in hand, we plotted similarity against distance for more than 31,000 pairs of glomeruli in the rat (**Fig. 8a**). At any given distance, we found about the same distribution of similarities. Even at the smallest distances there was no shortage of nearby glomeruli that had strongly differing or nonoverlapping response properties (**Figs. 5** and **7b**,**c**). The average similarity had almost no systematic dependence on distance (**Fig. 8a**).

If there were no chemotopic order on the bulb, then the distribution of similarities should be strictly identical at all interglomerular distances (**Fig. 8b**). We compared the observed distribution to this null hypothesis and resolved some small differences that reflected a weak trace of chemotopy (**Fig. 8c**): At short interglomerular distances <1 mm, comparable to the size of coarse odor domains, we found an excess of highly similar pairs and a dearth of dissimilar pairs. This excess was a small effect: It amounted to only 3.7% of all pairs of glomeruli separated by <1 mm and 1.7% of all glomerular pairs inspected. A second series of experiments, using a different odor set, reached the same conclusions (**Supplementary Fig. 5** online).

We repeated this analysis in the mouse with more than 33,000 pairs of glomeruli and it yielded very similar results (**Fig. 8d–f**). Again, similarity and distance were nearly independent of each other, with a small deviation at short distances; here, the excess amounted to 6.7% of glomerular pairs separated by <0.7 mm and 3% of all glomerular pairs considered. We concluded that on balance there is very little systematic mapping of glomeruli on a scale finer than the coarse domains. Furthermore, even the coarse domains do not impose a strong organization on the odor map. If one considers the response spectrum to a broad panel of odors, two glomeruli from the same domain, with <1 mm separation, are in most cases as dissimilar as those from different domains (**Fig. 8a**,**d**).

DISCUSSION

Our study was concerned with the functional anatomy of the olfactory bulb. We analyzed the spatial layout of glomeruli in relation to their odor sensitivity and found that many glomeruli could be identified uniquely and reliably by their odor sensitivity spectrum alone (**Figs. 3–5**). In both mouse and rat, the layout of glomeruli was notably precise, to within 0.6–1.6 glomerular spacings, and the variation was largest in the anterior-posterior direction (**Fig. 4** and **Table 1**). Some glomeruli appeared to be functionally identical in mouse and rat and were even located at corresponding positions on the bulb in both species (**Fig. 5**). There was only a coarse relationship between the odor

sensitivity of a glomerulus and its location on the bulb (**Fig. 6**). Nearby glomeruli tended to have very diverse odor sensitivities (**Figs. 5**, **7** and **8**). Here, we briefly discuss the basis for these conclusions and their implications.

Precision of the glomerular layout

By locating the corresponding glomeruli in different bulbs and superposing their layouts, we obtained both the mean location of each glomerulus and the variation about the mean (**Figs. 4** and **5**, and **Table 1**). We can picture this variation as arising from a developmental process that places each glomerulus at its 'intended' location modified by a random positioning error. In the mouse, that error region corresponded to a 1-s.d. ellipse containing ~1.8 glomeruli ($\pi \times 0.6 \times 0.95$; **Table 1**). Because the mouse bulb has ~1,800 glomeruli, this amounts to an impressive targeting precision of 1 part in 1,000. For the rat, the corresponding number was ~1 part in 500.

In contrast, several previous reports on this subject have emphasized the high variability of the glomeruli placement[7,11,12]. This discrepancy has two sources. First, some glomeruli seem to split into multiple copies and one prominent study[12] included the positions of several such duplicates in its estimate of variability. Our analysis was restricted to single glomeruli with a unique odor spectrum in the dorsal bulb. Second, some prior studies measured the absolute position of glomeruli with respect to anatomical landmarks[11,12], whereas we focused on the relative placement of glomeruli on the bulb surface. Any inter-individual variation in the global layout of the bulb, such as a slight shift or rotation, will affect the absolute coordinates, but for the logic of lateral interactions, only relative placement matters. A reanalysis of published data[11] confirms that the relative positions of glomeruli are in fact reproduced with high fidelity: For example, the medio-lateral displacement of two glomeruli (labeled Ea and Ma in Fig. S2 of ref. 11) varied across animals with a s.d. of only 88 μm, which compares well to our value of 95 μm (**Fig. 4c**). Another study[13] directly inspected the relative placement of two molecularly tagged glomeruli on the bulb and found that shifts by 1 or 2 array positions are most common, consistent with our results.

Coarse chemotopy and local diversity in the odor map

Chemotopy refers to the notion that chemically similar odors are mapped to nearby locations on the olfactory bulb. This idea faces some difficulty from the outset, as a single odor generally activates many olfactory receptors[26–28] and the glomeruli driven by those receptors tend to be loosely dispersed[10,14,19,29]. Our study confirmed this result. On average, a single odor stimulated 17 glomeruli spread over a region ~15 glomeruli in diameter in the rat (11 in an area ~14 glomeruli in diameter in the mouse; **Supplementary Fig. 6** online). The size of these regions of activation is much greater than the variability that we measured in glomerular positioning (s.d. of 1.6 or less; **Table 1**). Thus, the broad dispersion of glomeruli activated by a single odor is not caused simply by developmental noise in the odor map, but instead represents a reproducible feature of the map, and should not be ignored.

On the large scale of these single-odor patterns, the olfactory bulb does show a systematic chemotopic organization, in that certain chemically related odors tend to activate glomeruli in the same coarse domain of the bulb[17,18,20]. Two such domains on the dorsal bulb were apparent in our study: an anterior area responsive to aldehydes and a posterior area responsive to thiazoles (**Figs. 6b** and **7b**). These regions probably correspond to clusters A and D identified in ref. 20 and the domains for aldehydes and aromatic hydrocarbons in ref. 17. Notably, these two odor classes emerged here from an unbiased analysis that simply looked for a systematic odor map on the bulb, entirely blind to the identity of the odors (**Fig. 6b**). The map that we found was rather coarse: Knowing the odor spectrum of a glomerulus determined its position only to within ± 600 μm, comparable to the ~1-mm size of the reported odor domains. Again, the coarse resolution of the chemotopic map cannot be ascribed to developmental noise because the positioning of individual glomeruli was, in fact, much more precise (**Table 1**).

It has been suggested that there is local chemotopy on a fine scale in the odor domains and that certain structural features of odorants are mapped continuously across neighboring glomeruli[17,20,23]. We saw some indications of this, such as local clusters of glomeruli tuned to aliphatic aldehydes of different lengths (**Fig. 7a**). However, these structures are apparent only if one focuses on a specific molecular feature and ignores others. In general, glomeruli that are sensitive to one odor class tended to be interspersed by glomeruli that responded to entirely different odors (**Figs. 5** and **7b**), as seen in earlier studies[10,18,19,29]. The question arises how prevalent such local chemotopy really is and whether it can be assessed in an unbiased way that does not adjust the criteria to each neighborhood of glomeruli. For this purpose, we asked whether nearby glomeruli systematically have a similar odor sensitivity spectrum (**Fig. 8**). We found that the chemical similarity of two glomeruli was almost entirely independent of their proximity. A small enhanced similarity among nearby glomeruli decayed with distance on the scale of ~1 mm (**Fig. 8a**,**d**) and thus reflects the organization of the coarse odor domains. This departure from independence affected only a few glomerular pairs (rat, <4%; mouse, <7%). Thus, the dominant characteristic of the olfactory map seems to be local diversity: any mitral cell finds itself surrounded by glomeruli with many different odor sensitivity spectra. Because glomerular placement is so precise, this local diversity is a reliable feature rather than a random flaw of the odor map.

What does the olfactory bulb compute?

The basic circuit of the olfactory bulb follows a simple scheme. Many parallel excitatory pathways are linked by lateral inhibition[30]. In each glomerulus, the sensory afferents make excitatory synapses onto 25–50 mitral cells, which in turn send their axons to higher olfactory centers. These through-pathways interact via two networks of interneurons, in the glomerular layer[31] and in the external plexiform layer[32]. Both networks are predominantly inhibitory, although there is evidence for lateral excitation as well[31,33]. Therefore, the individual mitral cell receives excitation from receptor afferents in its primary glomerulus and potential contributions from other glomeruli in a large region extending to a 1–2-mm radius[32]. Clearly the nature of a mitral cell's computation depends on which of the surrounding glomeruli contribute and what odor signals they carry.

In one prominent proposal, the mitral cell collects inhibition from all glomeruli in a broad surrounding region, leading to a center-surround organization of sensitivity analogous to visual receptive fields in the retina[34]. Given the local diversity of odor spectra documented here, the glomeruli in such a broad surround region will collectively span a vast range of odor stimuli. If so, then lateral inhibition might implement a nonspecific gain control, such that any odor presented to the nose transiently lowers the sensitivity of all mitral cells. This could well serve for a rapid adaptation by which mitral cell processing becomes independent of absolute odor concentrations[35]. In contrast, such a nonspecific surround would not be useful for sharpening mitral cell sensitivity along a specific chemical axis[25].

In a very different scenario, a mitral cell collects inputs from just a small number of sparsely distributed glomeruli. In that case, the lateral circuits serve to perform a specific comparison of a few components of

the odor stimulus. Given the local diversity of odor spectra that we found among glomeruli, every mitral cell could perform a unique computation, even those neurons sharing the same principal glomerulus. There are some strong indications in favor of this theory. Nearby mitral cells do indeed have quite different odor sensitivity[36], especially with regard to their inhibitory inputs[37]. Anatomical tracing suggests that the lateral networks leading to individual mitral cells are sparse[38] and a comparison of mitral cell responses to those of surrounding glomeruli directly showed that the mitral cell collects a sparse set of inputs[39]. If each mitral cell indeed combines a different set of olfactory signals from the local field of glomeruli, then the number of different output channels of the bulb greatly exceeds the number of odorant receptors. This amounts to a substantial revision of how the olfactory bulb operates.

METHODS

Subjects. The animal subjects consisted of 11 adult rats (female Wistar or Long-Evans, ~300 g) and 12 adult mice (males and females, *Omp-SpH* heterozygous[40], >65 d old, 25–30 g). Each animal was prepared for surgery with atropine (25 μg per kg, intraperitoneal injection), anesthetized with urethane (12.5% intraperitoneal injection, final dose ~1.5 g per kg) or a cocktail of ketamine/xylazine (initial dose of either 100 or 10 mg per kg), and mounted in a stereotaxic frame. The skull was thinned or removed completely to reveal the dorsal surface of both olfactory bulbs. Low melting–point agarose (1.5%) was poured over the thinned bone and topped with a cover slip. All animal procedures conformed to US National Institutes of Health guidelines and were approved by Harvard University's Animal Care and Use Committee.

Stimulation. Odorants were delivered to the animal using either of two automated olfactometers (described in the **Supplementary Methods** online). For several odorants representing different chemical classes, we used a flame ionization detector to measure the final vapor concentration: typically 0.1–1% of the saturated vapor at 25 °C. These concentrations are low enough to avoid saturation of most receptors[10]. A list of all of the odors and the odor sets used in each figure are provided in **Supplementary Tables 1** and **2** online.

Imaging. An instrument was developed to measure intrinsic signals and SpH signals in parallel[41]. A dual illuminator, using bright light-emitting diodes, delivered either blue light (~470 nm for SpH, Luxeon V LED, Lumileds) or deep red light (~780 nm for intrinsic signal, Roithner Laser Technik) that was switched rapidly under computer control (**Fig. 1a**). Images were acquired with a CCD camera (Vosskühler 1300-D) at 12-bit resolution, with a frame rate of 25 frames per s (intrinsic signal) or 4 frames per s (SpH). Two photo lenses coupled front to front were used to image the olfactory bulb surface onto the CCD array, with a pixel size of 16 μm (mouse) or 20 μm (rat). Some intrinsic signal data were recorded in similar manner using an earlier acquisition system (Imager 2001, Optical Imaging).

Image acquisition typically began 20 s before odor delivery and continued for another 20 s during odor presentation. The interstimulus interval was 40–60 s of fresh air. Each stimulus was presented four to ten times, interleaved with other odor trials. For each odor, a ratio image was computed by dividing the average image during odor exposure by the image during the preceding air exposure. Signals were averaged further over trials with the same odor. For intrinsic signals, the ratio image was filtered to remove contamination from a large-scale hemodynamic signal[10] by subtracting a copy convolved with a Gaussian spatial kernel (s.d. = 330 μm).

Delivery of an odor often produced spots in the ratio image that corresponded to the activation of individual glomeruli[10,40]. For each distinct spot, the intensity profile was approximated with a two-dimensional Gaussian. The response strength of the glomerulus to any given odor was measured as the best-fit amplitude of its Gaussian to that odor's intrinsic image[10]. For display, we inverted the intrinsic signal images to show bright spots (**Figs. 1** and **3b** and **Supplementary Fig. 1**).

Comparison of intrinsic signal and SpH. The two optical probes, intrinsic signal and SpH, report neural activity via different mechanisms. By its design, the SpH reporter is linked to presynaptic release of transmitter from receptor neuron terminals[42]. The cellular origin of the intrinsic signal is somewhat less understood and there has been debate about whether its origins in the glomerulus are presynaptic or postsynaptic[43,44]. If there is a postsynaptic component from mitral cells or periglomerular cells, then the odor response recorded from a given glomerulus may include signals transmitted laterally from other glomeruli, which could alter the odor sensitivity spectrum. Therefore, we began by testing whether the two methods reported the same odor spectrum.

In recordings from mouse olfactory bulb, the illuminating light was switched rapidly every 3.2 s between blue (SpH) and red (intrinsic signal), allowing for interleaved measurement of both signals during the same odor response (**Fig. 1a**). Across a panel of 88 odors, about 70 glomeruli per bulb could be activated using SpH and a similar number could be activated using intrinsic signal (**Fig. 1b**).

By graphing the intensity of a single glomerulus for all the odors, we obtained a response spectrum. The spectra derived from SpH and intrinsic signal were often very similar (**Fig. 1c**), except that the SpH response was much larger than that of the intrinsic signal (**Fig. 1d**). Furthermore, this ratio between SpH and intrinsic signals varied greatly among glomeruli (range = ~10–60; **Fig. 1e**). After scaling the SpH and intrinsic signals of a given glomerulus for this relative gain, the two odor response spectra became indistinguishable. We measured their similarity by the correlation coefficient of the two signals (equation (1)). These correlations were very high (mean across glomeruli, 0.89 ± 0.01; **Fig. 1f**), indicating that, for the vast majority of glomeruli, the scaled SpH and intrinsic signal signals varied proportionally, at least over the odor conditions in our experiments.

The fact that SpH and intrinsic signals have different relative gain across glomeruli probably results from their distinct biophysical origins. For example, the SpH signal will be affected by the resting activity of receptor neurons, the ratio of synaptic to other membranes in the glomerulus and the amount of overlying nerve layer. Presumably such glomerulus-specific scaling of signals would also be beneficial in comparing intrinsic signal to intracellular calcium responses[40]. The fact that the two signals have identical odor dependence is consistent with prior suggestions that the intrinsic signal is strongly linked to presynaptic glutamate release, perhaps via the effects on nearby astrocytes[43]. For the present purpose, we take advantage of the fact that the normalized odor spectra are identical and use the two imaging methods interchangeably.

Matching glomerular response spectra. To formalize the matching of glomeruli that are driven by the same odorant receptor, we used a simple measure of similarity between two odorant spectra: the uncentered correlation coefficient among their two responses across the different odors,

$$s^{(A,B)} = \text{similarity of glomeruli } A \text{ and } B = \frac{\sum_{j=1}^{n} r_j^{(A)} r_j^{(B)}}{\sqrt{\sum_{j=1}^{n} r_j^{(A)} r_j^{(A)}} \cdot \sqrt{\sum_{j=1}^{n} r_j^{(B)} r_j^{(B)}}} \qquad \text{equation (1)}$$

where $r_j^{(A)}$ = response of glomerulus A to odor j, and n = number of odors. Two glomeruli with the same odorant sensitivity have a similarity of 1, whereas glomeruli that respond to nonoverlapping odor sets have a similarity of 0.

To match glomeruli in one bulb with those in another, we computed the similarity for every inter-bulbar pair. The pair with the highest similarity was accepted as being a match and was removed from consideration. This process was repeated until all possible pairings occurred. We tested more complex algorithms that optimize overall similarity over several simultaneous matches, but they always yielded results that were comparable to this simple serial method.

To reduce the effects of noise on this analysis, we set responses of very low amplitude (<0.002 for SpH or <0.00015 for intrinsic signal) to 0 (**Supplementary Fig. 7** online). Furthermore, to accept a match, we generally imposed two conditions: strong similarity (>0.75) and uniqueness (similarity > 0.05 for the next best match).

Alignment of maps. In comparing the layouts of glomeruli on two bulbs, we started with the two sets of locations of matched glomeruli. We reflected left

bulbs across the antero-posterior axis. We then shifted and rotated the first bulb to align optimally with the second bulb. Specifically, we minimized the squared distance between the locations of corresponding glomeruli, $\sum_{i=1}^{m} \left(\mathbf{x}^{(i)} - \mathbf{y}^{(i)}\right)^2$, where m is the number of matched glomeruli in each bulb, $\mathbf{x}^{(i)}$ is the location of glomerulus i in the first bulb after rotation and translation, and $\mathbf{y}^{(i)}$ is the location of glomerulus i in the other bulb. Subsequent analysis of this alignment focused on the residual shift vectors $\mathbf{x}^{(i)} - \mathbf{y}^{(i)}$ and their extent in the antero-posterior and medio-lateral directions.

In **Figure 4f**, we compared the layout of two bulbs to test whether nearby glomeruli suffered similar displacements. Consider an identified glomerulus i, with locations $\mathbf{x}^{(i)}$ and $\mathbf{y}^{(i)}$ in the two bulbs, and another glomerulus j, located at $\mathbf{x}^{(j)}$ and $\mathbf{y}^{(j)}$. We measured their separation vector in the first bulb, $\Delta\mathbf{x}^{(ij)} = \mathbf{x}^{(i)} - \mathbf{x}^{(j)}$, and their separation vector in the other bulb, $\Delta\mathbf{y}^{(ij)} = \mathbf{y}^{(i)} - \mathbf{y}^{(j)}$. The graph shows the relative displacement of the two glomeruli $\left|\Delta\mathbf{y}^{(ij)} - \Delta\mathbf{x}^{(ij)}\right|$ as a function of their separation $\left|\Delta\mathbf{x}^{(ij)}\right|$.

Prototype maps and matches across species. To find a set of canonical glomeruli in each species, we started with all glomeruli in eight mouse bulbs and four rat bulbs. The analysis was restricted to glomeruli whose odor spectrum could be matched to a glomerulus in another individual of the same species. We required this match to be both reliable (similarity > 0.75) and unique (>0.05 difference from second best match). We then subjected this set of glomeruli to a cluster analysis on the basis of the similarity between spectra (average linkage clustering, cutoff at similarity $= 0.75$). Each cluster with three or more members was taken to represent a canonical group of identical glomeruli. We averaged the location and the odor spectrum across members of the cluster (plotted in **Fig. 5**).

To identify functionally similar glomeruli across species, we paired the canonical glomeruli in mouse and rat using the same matching algorithm described for individual glomeruli. This strategy gave rise to ten pairs of canonical glomeruli with near identical function in the mouse and rat (**Fig. 5**). An alternate strategy revealed another six such shared glomeruli (**Supplementary Fig. 4**).

Linear map of spectrum to location. We performed a linear regression to find the best linear map between the odor response vector $\mathbf{r}$ and the glomerular position on the bulb $\mathbf{x}$:

$$\mathbf{x} \approx \mathbf{A} \cdot \mathbf{r}$$

where

$$\mathbf{x} = \begin{bmatrix} x_1 \\ x_2 \end{bmatrix} = \begin{bmatrix} \text{antero-posterior position} \\ \text{medio-lateral position} \end{bmatrix}$$

$$\mathbf{A} = \begin{bmatrix} A_{11} & \dots & A_{1n} \\ A_{22} & \dots & A_{2n} \end{bmatrix} = \text{matrix of map coefficients} \qquad \text{equation (2)}$$

$$\mathbf{r} = \begin{bmatrix} r_1 \\ \vdots \\ r_n \end{bmatrix} = \text{spectrum of responses to } n \text{ odors}$$

We first normalized each response vector $\mathbf{r}$ so that its components summed to unity, $\sum_{j=1}^{n} r_j = 1$. By doing this, two glomeruli with the same relative odorant sensitivity, but different overall response amplitude, will map to the same location. We then determined the matrix $\mathbf{A}$ to minimize the squared error, $\sum_{i=1}^{m} \left(\mathbf{x}^{(i)} - \mathbf{A} \cdot \mathbf{r}^{(i)}\right)^2$, where m is the number of glomeruli. When $n > m$, the problem is underdetermined, with more unknowns than measurements. Thus, we began by reducing the dimensionality of the odor response spectra. From the set of n-dimensional vectors $\mathbf{r}$, we determined the first five principal components, projected each $\mathbf{r}$ onto those directions and applied the fit to the resulting five-dimensional response vectors. For the analysis in **Figure 6**, the glomerular position in each bulb was measured relative to the average position of all observed glomeruli.

Similarity and distance for pairs of glomeruli. As a measure of functional similarity of two glomeruli (**Fig. 8**), we chose again the correlation of the two odor spectra $s^{(A,B)}$ (equation (1)). To retain maximal sensitivity to any local chemotopic order, we analyzed only pairs of glomeruli in the same olfactory bulb, which eliminates the effect of developmental variation across bulbs or individuals. For each pair, we plotted similarity versus distance between the centers of the two glomeruli and created a histogram of the result, yielding a joint probability distribution (**Fig. 8a**). By projecting this graph onto either axis, we obtained the marginal distributions of distance and of similarity. To test whether similarity and distance are at all related, we computed the product of the two marginal distributions (**Fig. 8b**). This product is the joint distribution expected under the null hypothesis that similarity and distance are statistically independent. Finally, we subtracted this expectation from the observed joint distribution (**Fig. 8c**) to highlight any deviations from independence (**Fig. 8c**).

Note: Supplementary information is available on the Nature Neuroscience website.

ACKNOWLEDGMENTS

We thank P. Mombaerts for providing M72-EGFP mice and R. Wilson and N. Uchida for healthy critiques.

AUTHOR CONTRIBUTIONS

E.R.S., D.F.A., V.N.M. and M.M. designed the study, E.R.S., D.F.A. and A.L.F. performed experiments and analysis, E.R.S., D.F.A. and M.M. wrote the manuscript, and V.N.M. and M.M. supervised the project.

Published online at http://www.nature.com/natureneuroscience/
Reprints and permissions information is available online at http://www.nature.com/reprintsandpermissions/

1. Kaas, J.H. Topographic maps are fundamental to sensory processing. *Brain Res. Bull.* **44**, 107–112 (1997).
2. Knudsen, E.I., du Lac, S. & Esterly, S.D. Computational maps in the brain. *Annu. Rev. Neurosci.* **10**, 41–65 (1987).
3. Chklovskii, D.B. & Koulakov, A.A. Maps in the brain: what can we learn from them? *Annu. Rev. Neurosci.* **27**, 369–392 (2004).
4. Serizawa, S., Miyamichi, K. & Sakano, H. One neuron–one receptor rule in the mouse olfactory system. *Trends Genet.* **20**, 648–653 (2004).
5. Mombaerts, P. Molecular biology of odorant receptors in vertebrates. *Annu. Rev. Neurosci.* **22**, 487–509 (1999).
6. Imai, T. & Sakano, H. Roles of odorant receptors in projecting axons in the mouse olfactory system. *Curr. Opin. Neurobiol.* **17**, 507–515 (2007).
7. Mombaerts, P. Axonal wiring in the mouse olfactory system. *Annu. Rev. Cell Dev. Biol.* **22**, 713–737 (2006).
8. Ressler, K.J., Sullivan, S.L. & Buck, L.B. Information coding in the olfactory system: evidence for a stereotyped and highly organized epitope map in the olfactory bulb. *Cell* **79**, 1245–1255 (1994).
9. Belluscio, L. & Katz, L.C. Symmetry, stereotypy, and topography of odorant representations in mouse olfactory bulbs. *J. Neurosci.* **21**, 2113–2122 (2001).
10. Meister, M. & Bonhoeffer, T. Tuning and topography in an odor map on the rat olfactory bulb. *J. Neurosci.* **21**, 1351–1360 (2001).
11. Oka, Y. *et al.* Odorant receptor map in the mouse olfactory bulb: *in vivo* sensitivity and specificity of receptor-defined glomeruli. *Neuron* **52**, 857–869 (2006).
12. Schaefer, M.L., Finger, T.E. & Restrepo, D. Variability of position of the P2 glomerulus within a map of the mouse olfactory bulb. *J. Comp. Neurol.* **436**, 351–362 (2001).
13. Strotmann, J. *et al.* Local permutations in the glomerular array of the mouse olfactory bulb. *J. Neurosci.* **20**, 6927–6938 (2000).
14. Wachowiak, M. & Cohen, L.B. Representation of odorants by receptor neuron input to the mouse olfactory bulb. *Neuron* **32**, 723–735 (2001).
15. Stewart, W.B., Kauer, J.S. & Shepherd, G.M. Functional organization of rat olfactory bulb analyzed by the 2-deoxyglucose method. *J. Comp. Neurol.* **185**, 715–734 (1979).
16. Johnson, B.A. *et al.* Functional mapping of the rat olfactory bulb using diverse odorants reveals modular responses to functional groups and hydrocarbon structural features. *J. Comp. Neurol.* **449**, 180–194 (2002).
17. Johnson, B.A. & Leon, M. Chemotopic odorant coding in a mammalian olfactory system. *J. Comp. Neurol.* **503**, 1–34 (2007).
18. Friedrich, R.W. & Korsching, S.I. Combinatorial and chemotopic odorant coding in the zebrafish olfactory bulb visualized by optical imaging. *Neuron* **18**, 737–752 (1997).
19. Uchida, N., Takahashi, Y.K., Tanifuji, M. & Mori, K. Odor maps in the mammalian olfactory bulb: domain organization and odorant structural features. *Nat. Neurosci.* **3**, 1035–1043 (2000).
20. Mori, K., Takahashi, Y.K., Igarashi, K.M. & Yamaguchi, M. Maps of odorant molecular features in the mammalian olfactory bulb. *Physiol. Rev.* **86**, 409–433 (2006).
21. Potter, S.M. *et al.* Structure and emergence of specific olfactory glomeruli in the mouse. *J. Neurosci.* **21**, 9713–9723 (2001).

22. Zhang, X., Zhang, X. & Firestein, S. Comparative genomics of odorant and pheromone receptor genes in rodents. *Genomics* **89**, 441–450 (2007).
23. Takahashi, Y.K., Kurosaki, M., Hirono, S. & Mori, K. Topographic representation of odorant molecular features in the rat olfactory bulb. *J. Neurophysiol.* **92**, 2413–2427 (2004).
24. Mori, K. & Shepherd, G.M. Emerging principles of molecular signal processing by mitral/tufted cells in the olfactory bulb. *Semin. Cell Biol.* **5**, 65–74 (1994).
25. Yokoi, M., Mori, K. & Nakanishi, S. Refinement of odor molecule tuning by dendrodendritic synaptic inhibition in the olfactory bulb. *Proc. Natl. Acad. Sci. USA* **92**, 3371–3375 (1995).
26. Duchamp, A., Revial, M.F., Holley, A. & MacLeod, P. Odor discrimination by frog olfactory receptors. *Chem. Senses* **1**, 213–233 (1974).
27. Malnic, B., Hirono, J., Sato, T. & Buck, L.B. Combinatorial receptor codes for odors. *Cell* **96**, 713–723 (1999).
28. Sicard, G. & Holley, A. Receptor cell responses to odorants: similarities and differences among odorants. *Brain Res.* **292**, 283–296 (1984).
29. Rubin, B.D. & Katz, L.C. Optical imaging of odorant representations in the mammalian olfactory bulb. *Neuron* **23**, 499–511 (1999).
30. Shepherd, G.M. & Greer, C.A. Olfactory bulb. in *The Synaptic Organization of the Brain* (ed. Shepherd, G.M.) 165–216 (Oxford University Press, Oxford, 2004).
31. Wachowiak, M. & Shipley, M.T. Coding and synaptic processing of sensory information in the glomerular layer of the olfactory bulb. *Semin. Cell Dev. Biol.* **17**, 411–423 (2006).
32. Egger, V. & Urban, N.N. Dynamic connectivity in the mitral cell–granule cell microcircuit. *Semin. Cell Dev. Biol.* **17**, 424–432 (2006).
33. Pimentel, D.O. & Margrie, T.W. Glutamatergic transmission and plasticity between olfactory bulb mitral cells. *J. Physiol. (Lond.)* **586**, 2107–2119 (2008).
34. Luo, M. & Katz, L.C. Response correlation maps of neurons in the mammalian olfactory bulb. *Neuron* **32**, 1165–1179 (2001).
35. Cleland, T.A., Johnson, B.A., Leon, M. & Linster, C. Relational representation in the olfactory system. *Proc. Natl. Acad. Sci. USA* **104**, 1953–1958 (2007).
36. Egana, J.I., Aylwin, M.L. & Maldonado, P.E. Odor response properties of neighboring mitral/tufted cells in the rat olfactory bulb. *Neuroscience* **134**, 1069–1080 (2005).
37. Buonviso, N. & Chaput, M.A. Response similarity to odors in olfactory bulb output cells presumed to be connected to the same glomerulus: electrophysiological study using simultaneous single-unit recordings. *J. Neurophysiol.* **63**, 447–454 (1990).
38. Willhite, D.C. *et al.* Viral tracing identifies distributed columnar organization in the olfactory bulb. *Proc. Natl. Acad. Sci. USA* **103**, 12592–12597 (2006).
39. Fantana, A.L., Soucy, E.R. & Meister, M. Rat olfactory bulb mitral cells receive sparse glomerular inputs. *Neuron* **59**, 802–814 (2008).
40. Bozza, T., McGann, J.P., Mombaerts, P. & Wachowiak, M. *In vivo* imaging of neuronal activity by targeted expression of a genetically encoded probe in the mouse. *Neuron* **42**, 9–21 (2004).
41. Albeanu, D.F., Soucy, E., Sato, T.F., Meister, M. & Murthy, V.N. LED arrays as cost effective and efficient light sources for widefield microscopy. *PLoS ONE* **3**, e2146 (2008).
42. Miesenböck, G., De Angelis, D.A. & Rothman, J.E. Visualizing secretion and synaptic transmission with pH-sensitive green fluorescent proteins. *Nature* **394**, 192–195 (1998).
43. Gurden, H., Uchida, N. & Mainen, Z.F. Sensory-evoked intrinsic optical signals in the olfactory bulb are coupled to glutamate release and uptake. *Neuron* **52**, 335–345 (2006).
44. Wachowiak, M. & Cohen, L.B. Correspondence between odorant-evoked patterns of receptor neuron input and intrinsic optical signals in the mouse olfactory bulb. *J. Neurophysiol.* **89**, 1623–1639 (2003).

Precision and diversity in an odor map on the olfactory bulb

Edward R. Soucy, Dinu F. Albeanu, Antoniu L. Fantana, Venkatesh N. Murthy,
and Markus Meister

Supplementary Material

Odor Stimulation

Odorants were diluted in mineral oil (1:100, typically), absorbed onto filter paper and stored in glass vials sealed with a thick rubber septum (Vacutainer™ #366431 tubes), grouped in a rack with 100 tubes. Two different machines were built to deliver odors from this set in arbitrary sequence under computer control. In one device, the rack was moved using two linear translators to position the desired tube under a pair of 20-gauge non-coring needles (Popper and Sons, Inc. #7184). A third translator pushed the needle assembly through the septum. Clean, filtered and humidified air entered through one needle, and the odor stream exited through the other needle at a rate of 1 L/min. In the other device, each tube had a permanent pair of needles through the septum, and the air flow was directed through the tube of choice by a network of solenoid valves and check valves. In either case, Teflon coated tubing carried the odorized air to the animal, through an anesthesia mask surrounding the animal's snout.

Nature Neuroscience: doi:10.1038/nn.2262

Supplementary Figure 1: Functional identification of glomeruli in rat

A. Maximum response projection map of intrinsic signal responses in the rat olfactory bulb: At each pixel the largest odor response is plotted in gray scale. Approximately 110 glomeruli could be stimulated on the dorsal surface of each bulb with a set of 100 odorants.
B. Sample odor response spectra of 5 pairs of glomeruli that were matched between the left and right bulbs of panel A. For odor identities, see Supplementary Table 1, Set A.
C. Locations of the best matches among glomeruli identified in the two bulbs of panel A.

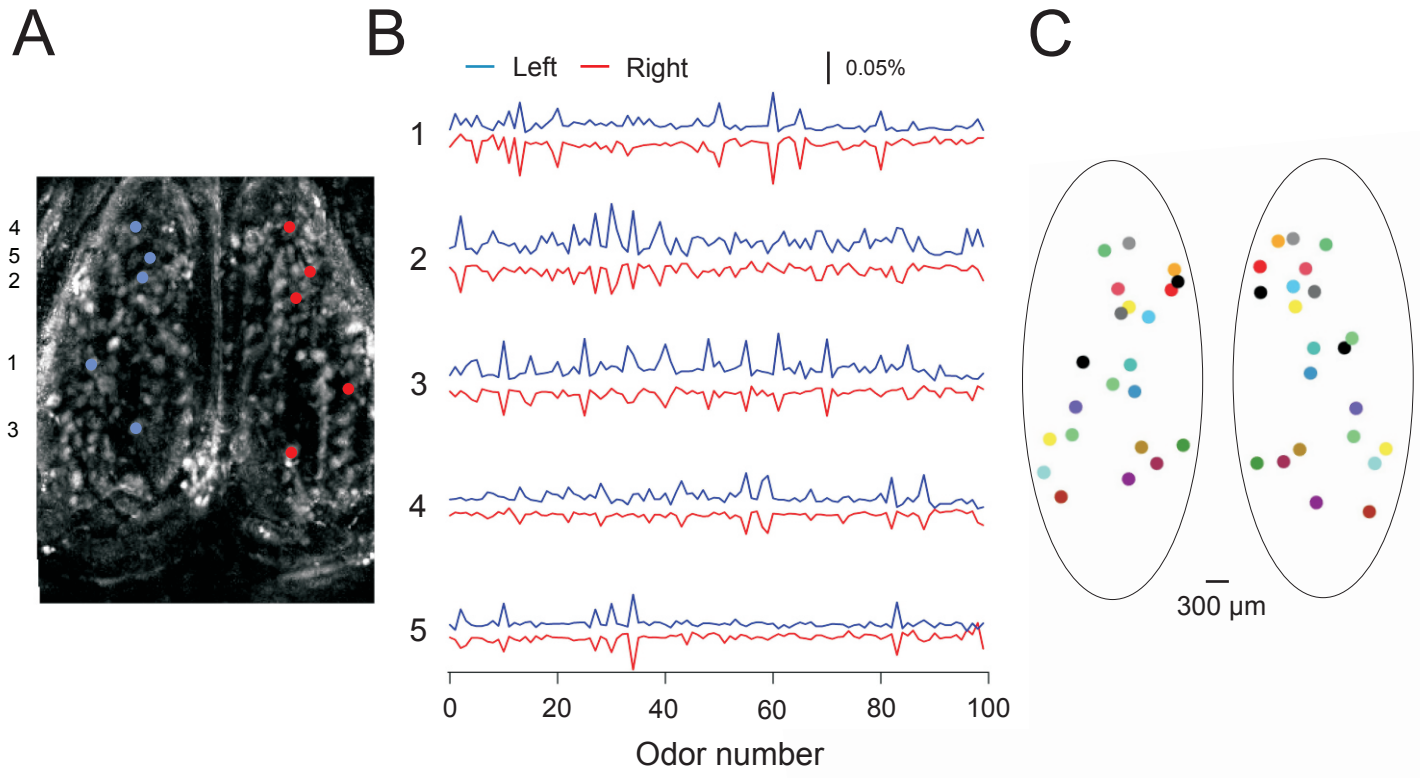

Supplementary Figure 2: Prototype map of the mouse olfactory bulb

A. Uniquely identifiable glomeruli on the dorsal surface of the right olfactory bulb in mouse. Each glomerulus is plotted at its average location. Glomeruli were included if they could be identified in at least 3 of 8 bulbs inspected.
B. The number of bulbs (of a total of 8) in which each prototype glomerulus was observed. The numerical labels were ordered so that glomeruli with low numbers occurred most frequently.
C. The average odor spectrum for each prototype glomerulus in panel A. For odor identities, see Supplementary Table 1, Set A.

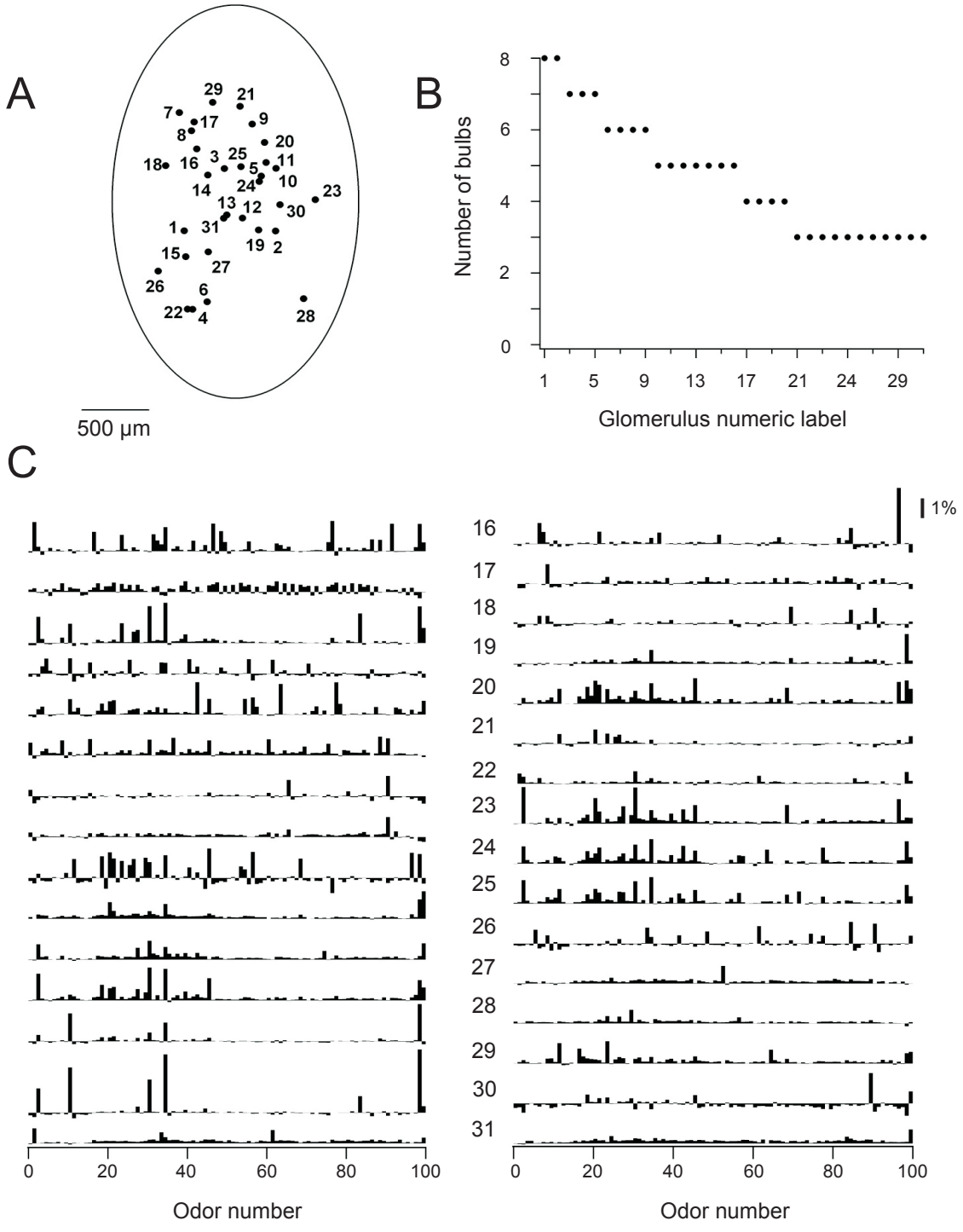

Supplementary Figure 3: Prototype map of the rat olfactory bulb

A. Uniquely identifiable glomeruli on the dorsal surface of the right olfactory bulb in rat, presented as in Supplementary Figure 2A. Glomeruli were included if they were identified in at least 3 of 4 bulbs inspected.
B. The average odor spectrum for each prototype glomerulus in panel A. For odor identities, see Supplementary Table 1, Set A.

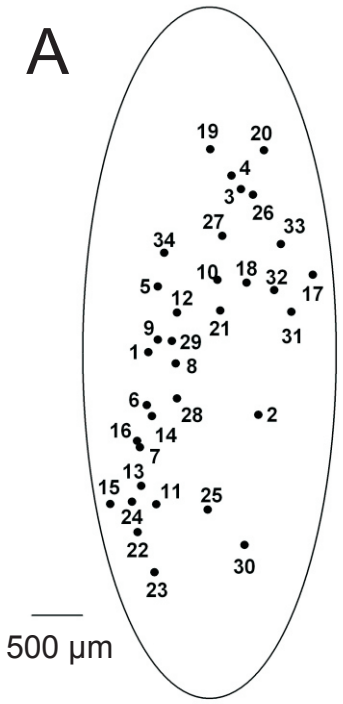

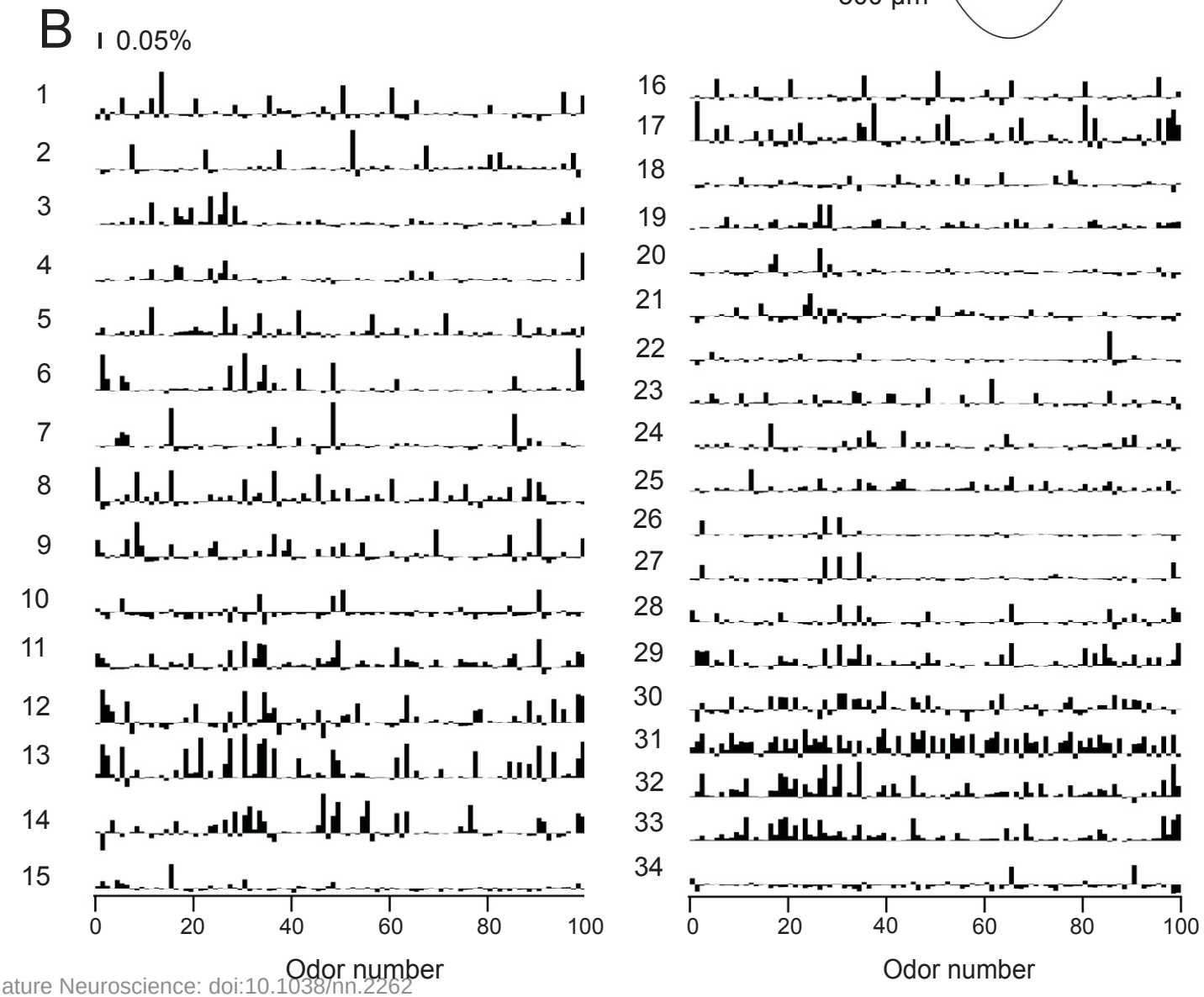

Nature Neuroscience: doi:10.1038/nn.2262

Supplementary Figure 4: Additional matches between glomeruli in mouse and rat

Odor spectra of glomeruli with strong similarity between mouse and rat. This analysis followed an alternate strategy to Fig 5: Glomeruli from individual mouse bulbs were compared directly with those from rat bulbs. All matches with similarity >0.75 were accepted. The resulting set of matching spectra was subjected to a cluster analysis (see Methods), and the average spectrum was computed for each cluster. From the resulting collection of spectra, those already identified in Fig 5 were removed, yielding the 6 additional spectra illustrated here. Scale bar refers to the SpH signal, the IS signal was scaled for easy comparison. For odor identities, see Supplementary Table 1, Set A.

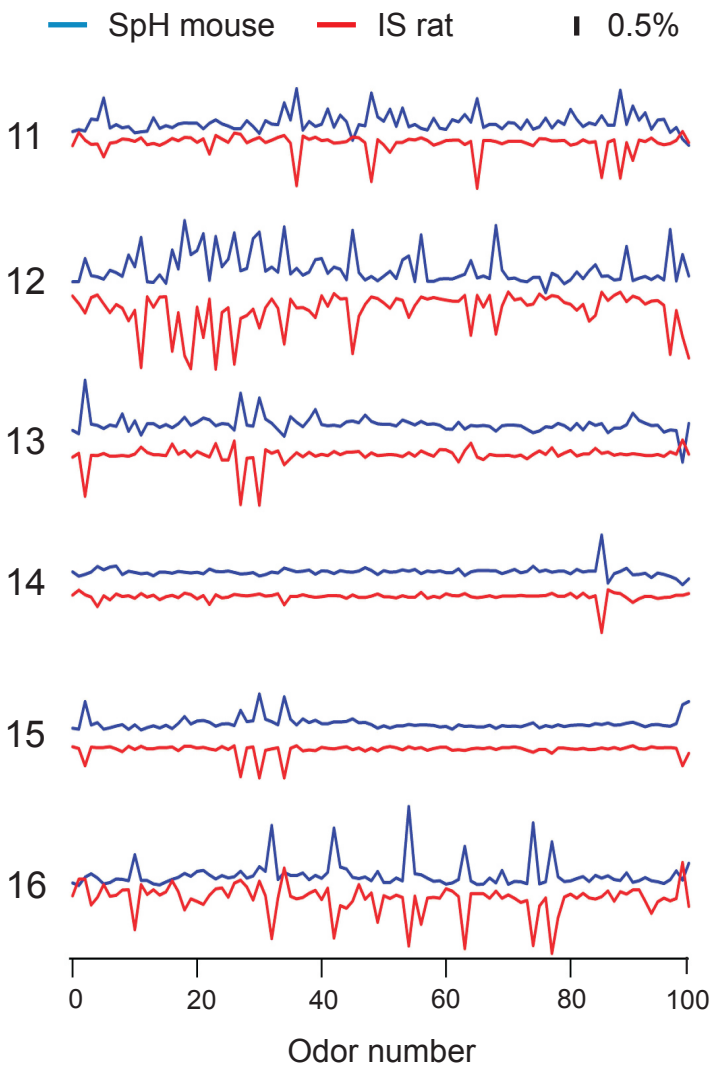

Supplementary Figure 5: Similarity vs distance for pairs of glomeruli on the rat olfactory bulb

We performed a second series of experiments to test for fine-scale chemotopy in the rat. The odor set (Supplementary Table 1, Set A) was different from that in Fig 8A-C, otherwise the analysis proceeded in the same fashion. As before, there is no significant dependence of similarity on inter-glomerular distance (C).

A. Relationship between the odor response similarity (ordinate, Eqn 1) of two glomeruli and their spatial separation (abscissa) in the rat. The analysis extended over 35,991 pairs of glomeruli in 6 olfactory bulbs from 3 rats. Each pair of glomeruli contributes one count in this histogram, and the gray scale reports the number of counts in each bin. Red lines: average (solid) and median (dashed) similarity vs. distance, obtained by binning the distance (150 pairs per bin). Green lines: average (solid) and median (dashed) distance vs. similarity, obtained by binning the similarity. If the response similarity had no dependence on distance, the red lines should be horizontal and the green lines vertical. For odor identities, see Supplementary Table 1, Set A.

B. Under the null hypothesis in which there is no chemotopy whatsoever, the response similarity of a pair of glomeruli should have the same probability distribution at all distances (see Methods). Therefore the joint distribution of similarity and distance should equal the product of the two marginal distributions. This prediction is plotted here; note the close resemblance to the measured distribution (panel A).

C. Difference between the measured distribution (panel A) and the distribution expected in absence of any chemotopy (panel B), plotted on an expanded grayscale. The region with the strongest deviation from the null hypothesis includes the pairs separated by <1 mm (vertical line) with similarity >0.6 (horizontal line): the excess there amounts to 2.4% of glomerular pairs separated by <1 mm or just 0.7% of all pairs.

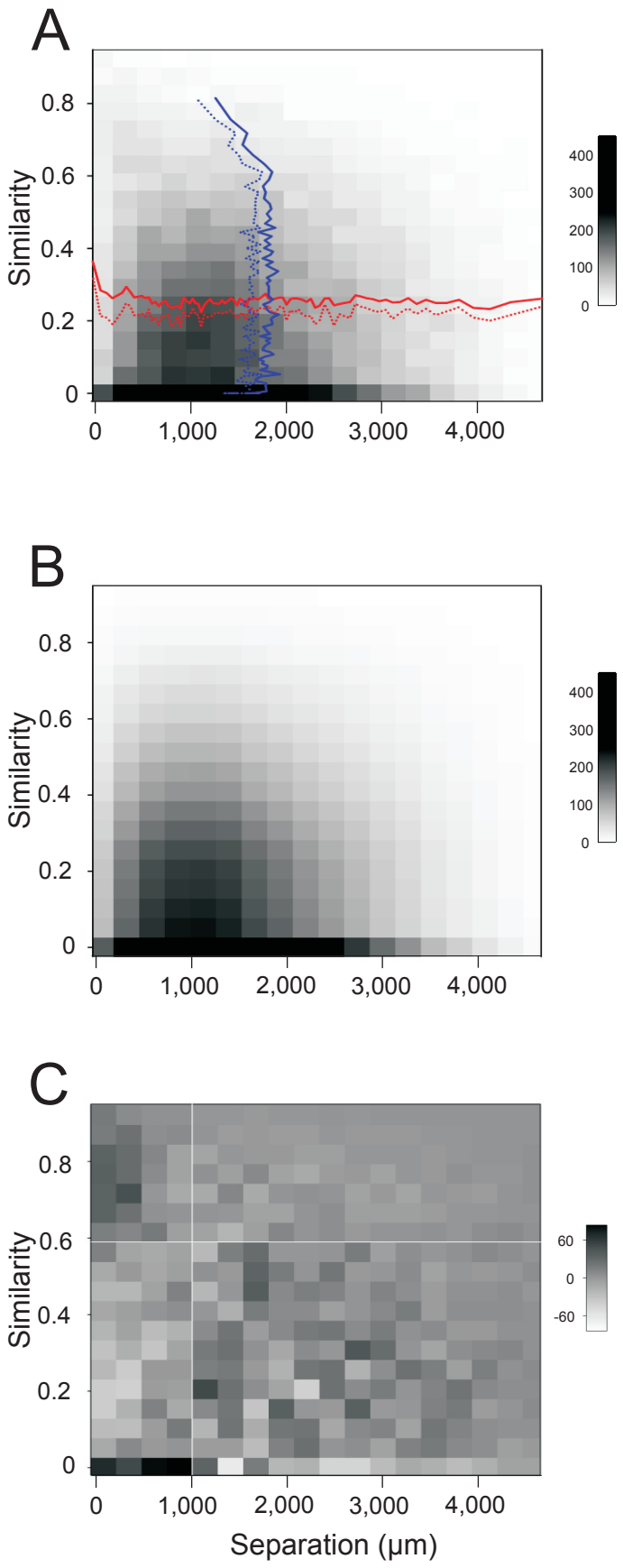

Nature Neuroscience: doi:10.1038/nn.2262

Supplementary Figure 6: The size of single-odor activation patterns

In general, a single odor activates a set of glomeruli sparsely scattered on the bulb. Here we measure the spatial extent of these activation patterns in mouse (A) and rat (B). For each odor, we identified the glomeruli activated above threshold (see Methods). Within that set, we computed the distribution of pairwise distances and averaged that distribution over all odors (solid bars). For reference, we draw the distribution expected if the activated glomeruli were distributed randomly inside a circle of diameter *D* (line; see Garwood, 1947, Biometrika 34, 1-17). By adjusting *D* to approximate the observed distribution, we estimate the size of the activated pattern. In the rat, the typical pattern involved 17 glomeruli in an area with a diameter of ~15 spacings; in the mouse 11 glomeruli in an area of diameter ~14 spacings. The analysis covered 8 olfactory bulbs in (A) and 6 in (B). For odor identities, see Supplementary Table 1, Set A.

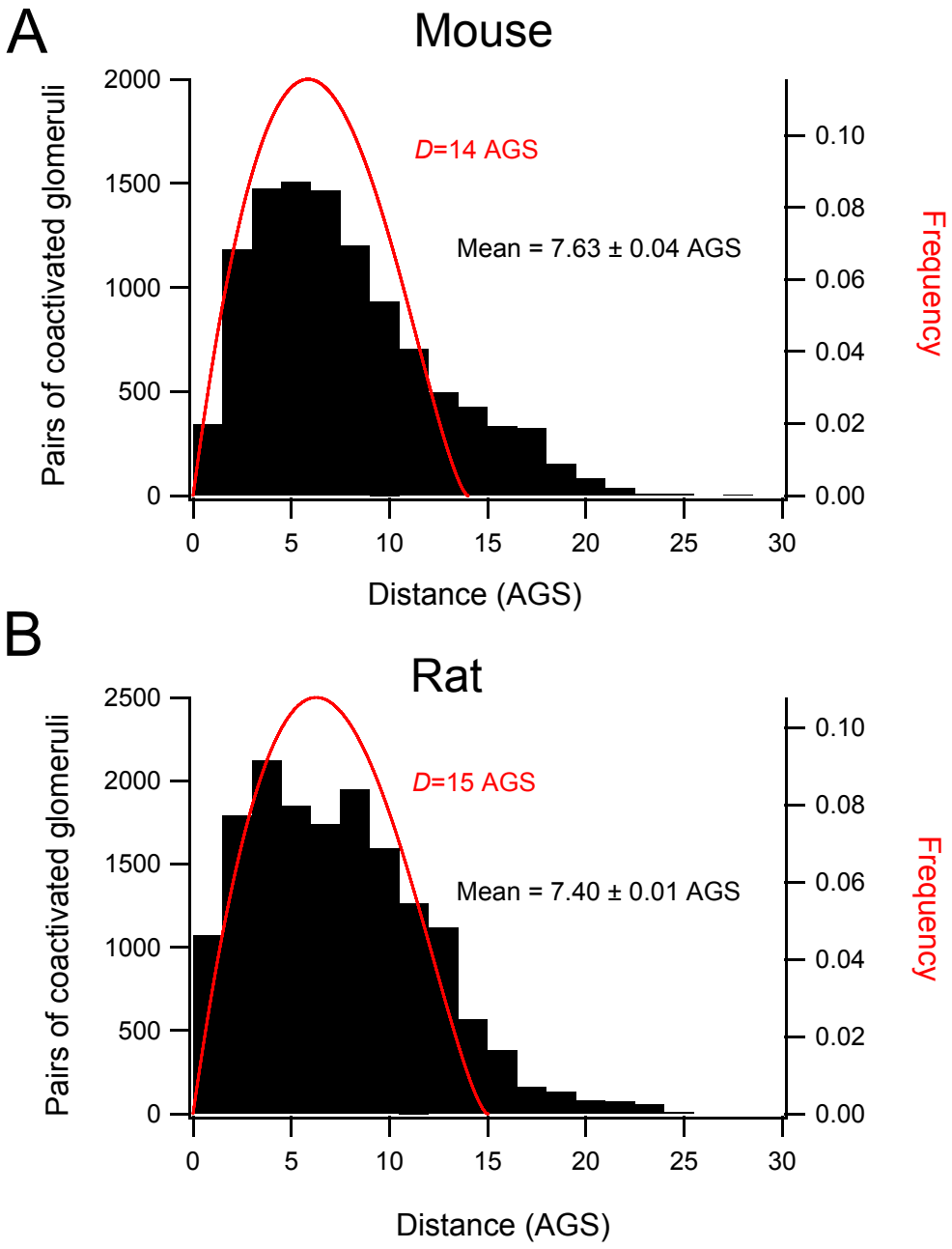

Supplementary Figure 7: Receiver Operating Characteristic (ROC) analysis determines a signal threshold

A. Maximum intensity projection map of SpH responses from olfactory bulbs in the mouse (see Figure 1B). Overt spots were taken to be glomeruli, and each of these was enclosed by a rectangular region of interest (ROI, e.g. sample white rectangle) used to measure its response amplitude with a Gaussian fit of the profile (see Methods). In addition, control ROIs were drawn in non-responsive regions of the dorsal bulb (black rectangles). The control ROIs were processed in the same way to yield response amplitudes caused by imaging noise.
B. For any given threshold value we counted the number of control regions whose amplitude exceeded threshold (false positives) and compared it to the number of bona fide glomeruli exceeding threshold (hits). We adopted a threshold of 0.002 which yielded a ratio of false positives to hits of ~10%. Signals below this threshold were set to zero. A similar analysis was applied to the IS responses.

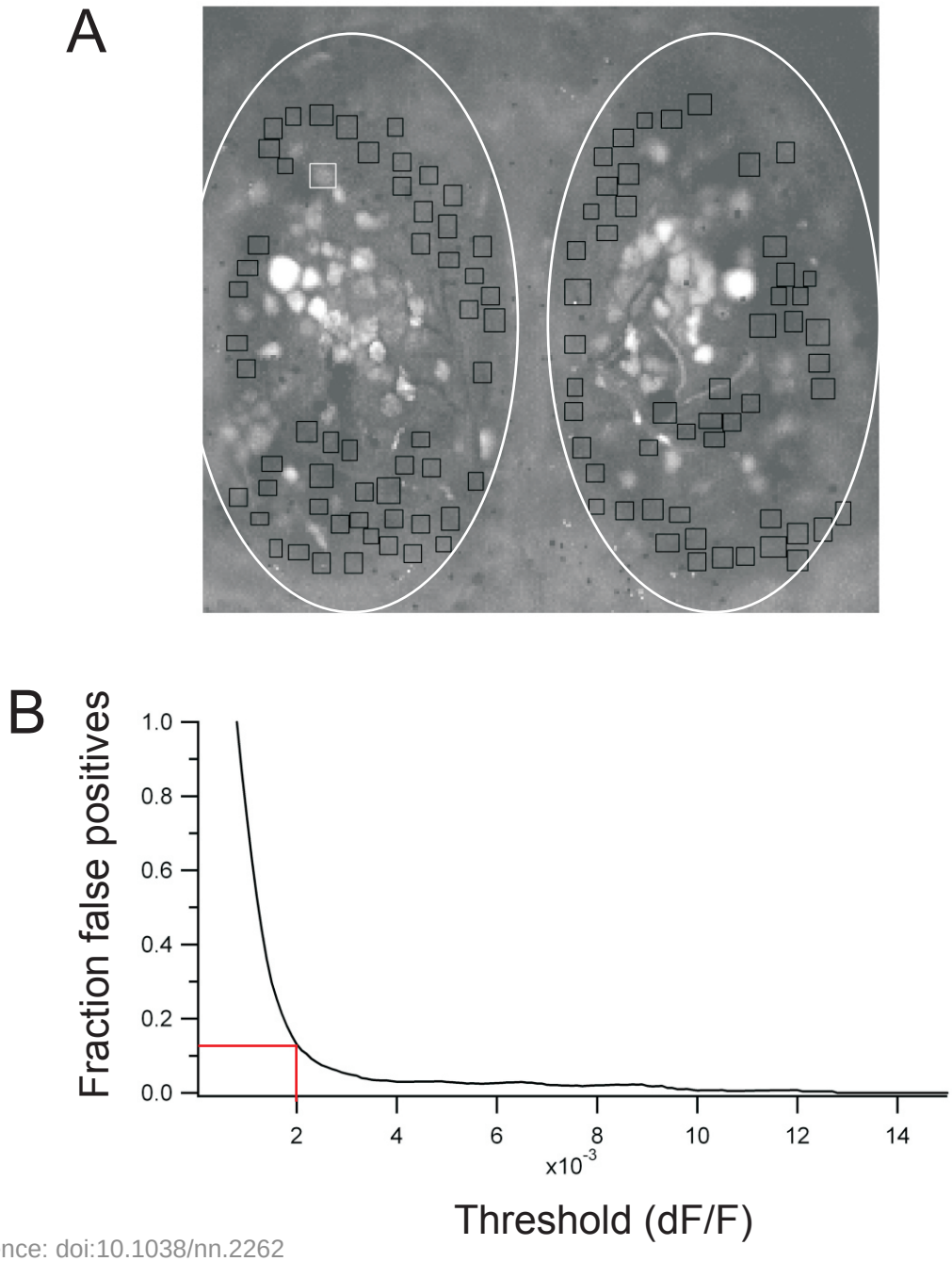

Nature Neuroscience: doi:10.1038/nn.2262

Supplementary Table 1: Reverse lookup list of all odors used

For each odor set, the odor number refers to the order of presentation during the experiment, and the value along the abscissa in the respective odor spectra. The odor index can be used to look up the corresponding odor name in Supplementary Table 2. For example, in Set A the substance presented at position 46 has odor index 11 and Supplementary Table 2 indicates this is 1-pentanol. In Set B, on the other hand, position 46 is a compound with odor index 206, which Supplementary Table 2 reveals to be methyl 2-pyrollyl ketone.

Odor number	Odor index					
	Set A	Set B	Set C	Set D	Set E	Set F
0	216	216	216	216	216	235
1	235	147	147	83	35	252
2	48	139	139	232	208	149
3	275	67	67	179	158	195
4	270	276	276	175	65	13
5	30	214	66	227	257	179
6	44	38	38	223	50	245
7	145	71	71	84	128	143
8	3	135	135	233	129	191
9	19	253	93	182	107	177
10	14	143	143	177	209	71
11	43	231	231	229	255	189
12	205	149	149	225	67	227
13	91	72	249	90	190	61
14	256	140	140	276	221	223
15	255	44	44	180	93	94
16	181	137	137	176	172	138
17	176	148	188	228	203	280
18	58	207	207	224	215	136
19	117	35	35	204	200	91
20	56	213	213	211	52	213
21	63	136	136	20	119	144
22	17	180	180	234	73	38
23	179	146	146	192	4	188
24	245	192	192	157	245	110
25	143	141	141	159	251	59
26	175	226	226	266	274	81
27	71	59	59	146	138	147
28	227	255	255	141	98	67
29	189	245	245	149	160	93
30	147	234	234	144	142	11
31	81	273	273	143	123	141
32	188	228	228	145	256	31
33	38	189	189	162	243	270

34	213	227	227	163	88	66
35	280	40	40	170	193	146
36	138	176	176	166	140	64
37	94	179	179	165	97	269
38	223	190	190	167	110	172
39	61	52	52	207	198	115
40	171	256	256	250	118	192
41	64	250	250	195	279	248
42	146	69	69	183	136	98
43	66	166	166	69	217	249
44	1	34	34	78	269	140
45	141	163	163	213	62	156
46	11	206	206	252	231	10
47	93	168	168	196	86	62
48	67	105	105	184	219	231
49	110	169	169	71	273	276
50	62	29	29	80	45	91
51	210	21	21	29	26	43
52	156	39	39	28	137	139
53	140	92	92	27	7	122
54	249	275	275	270	85	223
55	98	191	191	212	139	228
56	0	9	9	60	70	126
57	192	89	89	273	218	124
58	115	87	87	41	236	180
59	172	125	125	34	122	255
60	95	193	193	46	134	190
61	40	57	57	18	76	164
62	164	133	133	16	220	95
63	190	272	272	36	58	40
64	180	54	54	17	194	58
65	5	53	53	55	31	88
66	228	79	79	44	47	70
67	122	82	82	42	2	87
68	276	111	111	12	8	274
69	231	127	127	104	186	86
70	132	112	112	202	59	234
71	116	178	178	230	91	97
72	158	242	242	226	185	158
73	97	187	187	96	77	116
74	234	238	238	244	222	132
75	86	267	267	173	199	137
76	274	240	240	154	271	52
77	87	281	281	235	246	130
78	70	241	241	94	51	33

79	88	282	282	74	22	273
80	226	237	237	75	120	74
81	173	283	283	105	68	244
82	202	247	247	201	121	202
83	244	284	284	258	24	173
84	74	268	268	277	278	226
85	273	285	285	206	108	230
86	49		270	37	109	201
87	131		161	25	155	207
88	52			23	153	
89	137			15	152	
90	6			261	101	
91	68			260	99	
92	186			263	100	
93	254			262	103	
94	207			259	102	
95	201			265	114	
96	230			264	113	
97	174				106	
98	197				286	
99	150					

Supplementary Table 2: Alphabetical list of all odors used

The odor index listed here is used to reference odors in Supplementary Table 1. The odor number refers to the position on the abscissa in the response spectra illustrated in various figures. It also reflects the order of odor presentations during the experiment. Six different odor sets (A-F) were used in various parts of the study, as identified in the respective figure legends. For example, 1-pentanol has odor index 11 in this table and was presented at position 46 in Set A, at position 30 in Set F but was not used in Sets B, C, D, or E.

Odor index	Odor name	Odor number					
		Set A	Set B	Set C	Set D	Set E	Set F
0	1-propanethiol	56					
1	2-butenol	44					
2	2-pentanol					67	
3	4-allyl anisole	8					
4	1,1-diethoxyethane					23	
5	1,3- dimethoxy-benzene	65					
6	1,4 dimethoxy benzene	90					
7	1-butanethiol					53	
8	1-decanol					68	
9	1-heptanol		56	56			
10	1-methyl pyrrole						46
11	1-pentanol	46					30
12	2 isobutyl 3 methyl pyrazine				68		
13	2,3 ethyl pyrazine						4
14	2,3 pentane dione	10					
15	2,3,5,6 tetramethyl pyrazine				89		
16	2,3,5-trimethyl pyrazine				62		
17	2,3-diethyl pyrazine	22			64		
18	2,3-dimethyl pyrazine				61		
19	2,4 decadienal	9					
20	2,5- dimethyl pyrazine				21		
21	2,5-dimethyl thiazole		51	51			
22	2,5-dimethyl phenol					79	
23	2,6- dimethyl pyrazine				88		
24	2,6-dimethyl phenol					83	
25	2-acetyl pyrazine				87		
26	2-acetyl furan					51	
27	2-acetyl pyridine				53		
28	2-acetyl thiazole				52		

29	2-acetyl thiophene		50	50	51		
30	2-acetyl thiophenone	5					
31	2-butanol					65	32
32	2-butenol						
33	2-butyl cyclohexanone						78
34	2-ethoxy thiazole		44	44	59		
35	2-ethyl butyric acid		19	19		1	
36	2-ethyl pyrazine				63		
37	2-furyl methyl ketone				86		
38	2-heptanone	33	6	6			22
39	2-hexanal, trans		52	52			
40	2-hexanone	61	35	35			63
41	2-isobutyl thiazole				58		
42	2-methoxy 3-methyl pyrazine				67		
43	2-methoxy naftalene	11					51
44	2-methoxy pyrazine	6	15	15	66		
45	2-methoxy phenol					50	
46	2-methyl pyrazine				60		
47	2-octenal (E)					66	
48	2-propyl tiglate	2					
49	2-secbutyl cyclohexanone	86					
50	2-undecanone					6	
51	3,4-dimethoxy acetophenone					78	
52	3-acetyl 2,5-dimethyl furan	88	39	39		20	76
53	3-acetyl furan (solid)		65	65			
54	3-ethoxy, 4-hydroxy benzaldehyde		64	64			
55	3-ethyl 2-methyl pyrazine				65		
56	3-ethyl valerate	20					
57	3-hexanone		61	61			
58	3-methyl 2-buten 1-ol	18				63	64
59	4'-methoxy acetophenone (solid)		27	27		70	25
60	4,5-dimethyl thiazole				56		
61	4-heptanone	39					13
62	4-isopropyl benzaldehyde	50				45	47
63	4-propyl butyrate	21					
64	5 hydroxyethyl 4-methyl thiazole	41					36

65	5,6,7,8-tetrahydroquinoxaline					4	
66	acetal	43		5			34
67	acetophenone	48	3	3		12	28
68	acetovanillone	91				81	
69	allyl butyrate		42	42	43		
70	allyl cyclohexyl propionate	78				56	66
71	allyl tiglate	27	7	7	49		10
72	allyl tiglate (12%)		13				
73	ammonium sulfide					22	
74	anise oil (10%)	84			79		80
75	apple flavor				80		
76	benzaldehyde					61	
77	benzoic acid					73	
78	benzyl butyrate				44		
79	benzyl propionate		66	66			
80	benzyl tiglate				50		
81	benzyl trans 2-methyl 2-butenoate	31					26
82	bicyclononanal lactone		67	67			
83	butanal				1		
84	butanol				7		
85	butyl acetate					54	
86	butyl formate	75				47	69
87	butyl propionate	77	58	58			67
88	butyl sulfide	79				34	65
89	butylamine		57	57			
90	butyrate				13		
91	camphor	13				71	19
92	carvone		53	53			
93	carvyl acetate	47		9		15	29
94	cedarwood oil (10%)	37			78		15
95	cineole	60					62
96	cinnamon oil (10%)				73		
97	citral cis + trans	73				37	71
98	citronellal	55				28	42
99	citrus arantium					91	
100	citrus arantium v.amara					92	
101	citrus arantium v. bergamia					90	

102	citrus limon					94	
103	citrus reticulata v. mandarin					93	
104	clove oil (10%)				69		
105	coffee (10%)		48	48	81		
106	cupressus sempervirens					97	
107	cyclohexanone					9	
108	cyclohexanone / butylacetate					85	
109	cyclohexanone / butyrolactone					86	
110	cyclohexyl acetate	49				38	24
111	cyclohexyl ethyl acetate		68	68			
112	cyclohexyl ethyl alcohol		70	70			
113	cymbogom martini					96	
114	cymbogom nardus					95	
115	DBE-dibasic ester	58					39
116	decanolactone	71					73
117	decyl alcohol	19					
118	delta-decalactone					40	
119	delta-dodecalactone					21	
120	dextro-camphene					80	
121	dibenzyl disulfide					82	
122	diethyl maleate	67				59	53
123	difurfuryl disulfide					31	
124	dimethoxy acetophenone						57
125	dimethoxy benzaldehyde (solid)		59	59			
126	dimethoxy benzene						56
127	dimethyl benzyl carbonyl acetate		69	69			
128	dimethyl succinate					7	
129	dipropyl ketone					8	
130	dodecen acetate						77
131	dodecyl acetate	87					
132	dyhidrocarvone	70					74
133	dymethyl phenol (solid)		62	62			
134	estragole					60	
135	ethyl 2-mercaptopropionate		8	8			
136	ethyl 2-methyl butyrate		21	21		42	18
137	ethyl 3-hydroxy butyrate	89	16	16		52	75

138	ethyl 3-mercaptopropionate	36				27	16
139	ethyl acrylate		2	2		55	52
140	ethyl benzoylacetate	53	14	14		36	44
141	ethyl butyrate	45	25	25	28		31
142	ethyl formate					30	
143	ethyl heptanoate	25	10	10	31		7
144	ethyl hexanoate				30		21
145	ethyl octanoate	7			32		
146	ethyl propionate	42	23	23	27		35
147	ethyl tiglate	30	1	1			27
148	ethyl tiglate (1.6%)		17				
149	ethyl valerate		12	12	29		2
150	ethyl valerate 12%	99					
151	ethyl-benzyl-acetate						
152	eucalyptus citriodora					89	
153	eucalyptus globulus					88	
154	eucalyptus oil (10%)				76		
155	eucalyptus staigerana (natural oil)					87	
156	eugenol	52					45
157	farnesene				24		
158	fenchone (-)	72				3	72
159	filter paper (no mineral oil control)				25		
160	formic acid					29	
161	fox anal gland extract			87			
162	furfuryl proprionate				33		
163	furfuryl butyrate		45	45	34		
164	furfuryl disulfide	62					61
165	furfuryl heptanoate				37		
166	furfuryl hexanoate		43	43	36		
167	furfuryl octanoate				38		
168	furfuryl pentanoate		47	47			
169	furfuryl propionate		49	49			
170	furfuryl valerate				35		
171	gamma terpinene	40					
172	geraniol	59				16	38
173	ginger oil (10%)	81			75		83
174	hanoki oil (10%)	97					

175	heptanal	26			4		
176	heptanoic acid	17	36	36	16		
177	heptanol				10		9
178	hexalon		71	71			
179	hexanal	23	37	37	3		5
180	hexanoate	64	22	22	15		58
181	hexanoate (1/200)	16					
182	hexanol				9		
183	hexyl butyrate				42		
184	hexyl tiglate				48		
185	hydroquinone dimethyl ether					72	
186	indole	92				69	
187	ionone beta		73	73			
188	isoamyl acetate	32		17			23
189	isoamylamine	29	33	33			11
190	isobutyl propionate	63	38	38		13	60
191	isobutyl thiazole		55	55			8
192	isobutylamine	57	24	24	23		40
193	isoeugenol		60	60		35	
194	isoheptanol					64	
195	isopropyl butyrate				41		3
196	isopropyl tiglate				47		
197	isopropyl tiglate (12%)	98					
198	L-(-)-carvone					39	
199	L-menthol					75	
200	L-verbenone					19	
201	lavender oil (10%)	95			82		86
202	lemon oil (10%)	82			70		82
203	m-dimethoxy benzene					17	
204	meister bräu beer				19		
205	methoxy acetophenone	12					
206	methyl 2-pyrrollyl ketone solid		46	46	85		
207	methyl butyrate	94	18	18	39		87
208	methyl n-amyl ketone					2	
209	methyl propyl disulfide					10	
210	methyl pyruvate	51					
211	methyl sulfoxide				20		

212	methyl thiazole				55		
213	methyl tiglate	34	20	20	45		20
214	methyl tiglate (12%)		5				
215	methyl pyrrole					18	
216	mineral oil	0	0	0	0	0	
217	n-butyl propionate					43	
218	n-butylamine					57	
219	n-butyrophenone					48	
220	n-hexanoic acid					62	
221	n-propyl acetate					14	
222	naphthalene					74	
223	nonanal	38			6		14
224	nonanoic acid				18		
225	nonanol				12		
226	nutmeg oil (10%)	80	26	26	72		84
227	octanal	28	34	34	5		12
228	octanoic acid	66	32	32	17		55
229	octanol				11		
230	orange oil (10%)	96			71		85
231	p-anis aldehyde	69	11	11		46	48
232	pentanal				2		
233	pentanol				8		
234	pentyl acetate	74	30	30	22		70
235	peppermint oil (10%)	1			77		0
236	phenethylamine					58	
237	phenoxy ethyl isobutyrate		80	80			
238	phenoxy ethyl propionate		74	74			
239	phenyl acetate						
240	phenyl ethyl acetate		76	76			
241	phenyl ethyl alcohol		78	78			
242	phenyl ethyl isobutyrate		72	72			
243	phenyl mercaptan					33	
244	pine oil (10%)	83			74		81
245	piperidine	24	29	29		24	6
246	piperine					77	
247	prenyl acetate		82	82			
248	propane thiol						41
249	propyl acetate	54		13			43

250	propyl butyrate		41	41	40		
251	propyl mercaptan					25	
252	propyl tiglate				46		1
253	propyl tiglate (12%)		9				
254	pyrazine	93					
255	pyridine	15	28	28		11	59
256	pyrrolidine	14	40	40		32	
257	quinoline					5	
258	rose oil (10%)				83		
259	sigma cocaine scent				94		
260	sigma corpse 2				91		
261	sigma corpse 1				90		
262	sigma explosive scent				93		
263	sigma heroin scent				92		
264	sigma LSD scent				96		
265	sigma marijuana scent				95		
266	soiled bedding				26		
267	strawberriff		75	75			
268	styralyl propionate		84	84			
269	terpinene					44	37
270	thiazole	4		86	54		33
271	thymol					76	
272	tislic acid - isobutyl ester		63	63			
273	trimethyl thiazole	85	31	31	57	49	79
274	undecane	76				26	68
275	valeraldehyde	3	54	54			
276	valeric acid	68	4	4	14		49
277	vanilla butternut flavor				84		
278	veratraldehyde					84	
279	veratrole					41	
280	verbenone	35					17
281	verdox HC		77	77			
282	verdural B extra		79	79			
283	verdural extra		81	81			
284	vertenex		83	83			
285	vertenex HC		85	85			
286	vetiveria zizanioides					98	